JOURNAL OF COMPUTATIONAL PHYSICS 22, 34–73 (1976)

A Direct Numerical Approach to Three Nucleon Bound State Problems

I. M. BASSETT, B. R. E. LEDERER, AND G. C. VORLICEK

School of Physics, The University of Sydney, Sydney, New South Wales, 2006, Australia

Received September 8, 1975; revised January 19, 1976

This paper describes a direct numerical method for solving three nucleon bound state problems. The method has been tried out and developed on a sequence of two and three nucleon problems of increasing difficulty. This work forms part of an attack on the problem of calculating the triton binding energy with the nucleon–nucleon interaction described by the Hamada–Johnston potential. The method uses the analysis of Derrick and Blatt which reduces Schrödinger's equation for the ground state of the triton to an eigenvalue–eigenfunction problem consisting of a set of linked partial differential equations in three variables. In the main calculation described the full three nucleon ground state problem is simplified in two respects. Firstly, the spin orbit forces are omitted from the potential leaving only central and tensor forces. Secondly, in the expansion of the ground state wavefunction in terms of states of definite total angular momentum, iso-spin, and parity, only nine of the 16 components are included resulting in a problem involving nine partial-differential equations. A direct numerical approach is employed in which functions of three variables are represented by three-dimensional tables of numbers and derivatives by finite-difference operators. The numerical problem is thus obtained in the form of an eigenvalue–eigenvector problem. It is solved on a sequence of mesh sizes and an approximation to the analytic binding energy obtained by extrapolating to zero mesh size.

1. INTRODUCTION AND OUTLINE

An outstanding problem in nuclear physics is calculating the binding energy of the triton (a nucleus containing two neutrons and a proton), i.e., calculating how much energy is needed to effect an infinite separation of the three nuclear particles or nucleons. Three nucleon calculations may be useful in clarifying uncertainties in potentials representing the internucleon force and in deciding the importance of three body forces and relativistic effects [1–3]. Regarded as a test of a two-nucleon potential, a calculation of the triton binding energy is however ambiguous in that it is unclear whether any discrepancy found between the calculated binding energy and the experimental binding energy (−8.48 MeV) should be attributed to defects

in the potential or else to the effects of three body forces and relativity which are of uncertain magnitude and may be as large as 2 MeV [3]. In addition to ambiguities of this kind there are also ambiguities due to approximations of uncertain magnitude made in the calculations. The work described here was motivated by the desire to perform a calculation with a realistic potential that was free of the latter type of ambiguity. That this type of ambiguity is present in existing calculations with realistic potentials is clearly shown by recent triton binding energy results for the Reid potential [4] obtained with variational methods or methods based on the Faddeev equations [5–13].

In a recent review of current binding energy results for the Reid potential, Levinger favors a result of 7.1 MeV but finds it hard to estimate the uncertainty [38]. In the case of the Hamada–Johnston potential [14] two results have been obtained using variational methods: Delves *et al.* [15] found a binding energy of -6.5 MeV with an estimate of the accuracy of the calculation of ± 0.2 MeV, and Chi-yu Hu [16] found a binding energy of -6.7 MeV (with no estimate of the accuracy reported).

The method described in this paper is based on a direct finite-difference representation of Schrödinger's wave equation for the triton, whereby the hamiltonian operator is represented by a large (but sparse) finite matrix, whose dimension depends on the mesh size h. The problem of determining the binding energy becomes that of determining the appropriate eigenvalue of this matrix. The eigenvalue is a function of h and by determining it for a number of values of h an improved estimate of the binding energy may be made by extrapolation to $h = 0$. This method has been tried out on a series of problems of increasing difficulty [17, 18]: the ground state of the deuteron with firstly an exponential potential well with hard core and with secondly the Hamada–Johnston potential; and the ground state of the triton with firstly a central potential with hard core proposed by Ohmura [19] (henceforward referred to as "the S state problem") and with secondly the Hamada–Johnston potential with the central and tensor forces included but with the spin-orbit forces excluded (henceforward referred to as the "central and tensor problem"). The accuracy obtained for the binding energy in these problems is about six, four, five, and one figure, respectively. The application of the method to the full triton problem including spin-orbit forces in the Hamada–Johnston potential met with difficulties that have not all been overcome [20]. Nevertheless, the results of this paper indicate that direct methods are feasible for three nucleon problems and that the pessimism sometimes expressed about direct methods is unwarranted [21]. The S state calculation demonstrates that results of high accuracy can be obtained. The central and tensor calculation demonstrates that for a problem having the magnitude and complexity of the realistic problem including spin-orbit forces, one can obtain a result of sufficient accuracy to warrant comparison with other methods.

A. *The Derrick–Blatt Analysis*

Before adopting a finite-difference representation, the triton wave equation is reduced to a set of linked partial-differential equations in three variables by using the analysis of Derrick and Blatt. The wave equation may be written in cartesian coordinates in the form

$$[(-\hbar^2/2M)(\nabla_1^2 + \nabla_2^2 + \nabla_3^2) + V_{23} + V_{31} + V_{12}]\,\Psi = E\Psi. \tag{1}$$

The fundamental eigenvalue E is the binding energy of the nucleus. The wavefunction Ψ is a function of nine cartesian coordinates as well as the spins and isospins of the individual particles. ∇_i^2 is the Laplacian in three cartesian coordinates belonging to the ith particle. $-(\hbar^2/2M)(\nabla_1^2 + \nabla_2^2 + \nabla_3^2)$ is the kinetic energy operator, V_{ij} is the potential energy of interaction of particles i and j. In the case of the Hamada–Johnston potential (Section 2C) V_{ij} includes central forces as well as noncentral forces of tensor, spin-orbit, and quadratic spin-orbit type. The spin-orbit forces are excluded in the central and tensor calculation. The operator on the left of (1) is symmetric under the following operations: translation, rotation in ordinary space and in charge (isospin) space, inversion, permutation of particles, and hermitian conjugation. These symmetries are used to reduce (1) and are preserved in the numerical representation. The Derrick–Blatt analysis [22–24] shows that in the presence of noncentral forces the triton ground state wavefunction is composed of four spectroscopic components $^2S_{1/2}$, $^2P_{1/2}$, $^4P_{1/2}$, and $^4D_{1/2}$, comprising sixteen states Y_l of total angular momentum $J = \frac{1}{2}$, parity $\pi = +$, and total isospin $T = \frac{1}{2}$, as shown in Table I.

The Y_l are simultaneously eigenfunctions of the square of the orbital angular momentum, L^2, the square of the spin, S^2, and have well-defined symmetry with respect to permutations. Three types of permutation symmetry occur, corresponding to the three irreducible representations of the permutation group on three objects [25]: symmetric functions Y_s, antisymmetric functions Y_a, and pairs of functions of mixed symmetry (Y_{m_1}, Y_{m_2}). Under the action of the permutation operator P_{23} interchanging particles 2 and 3, for example, these functions transform as

$$\begin{aligned} P_{23}Y_s &= Y_s, \\ P_{23}Y_a &= -Y_a, \\ P_{23}Y_{m_1} &= -\tfrac{1}{2}Y_{m_1} + \tfrac{1}{2}3^{1/2}Y_{m_2}, \\ P_{23}Y_{m_2} &= \tfrac{1}{2}3^{1/2}Y_{m_1} + \tfrac{1}{2}Y_{m_2}. \end{aligned} \tag{2}$$

Two sets of D states have been defined by Derrick, an irregular and orthogonal set [22] and a regular and nonorthogonal set [24], and for the present calculation the latter set (shown in Table I) is chosen for reasons to be explained below (Section

TABLE I

Classification of Triton Wavefunctions Using the Regular and Nonorthogonal D States of [24]

Spectroscopic classification	State number l	L	S	Permutation symmetry Y_l	f_l
$^2S_{1/2}$	1	0	1/2	a	s
	2	0	1/2	s	a
	3	0	1/2	m_1	$-m_2$
	4	0	1/2	m_2	m_1
$^2P_{1/2}$	5	1	1/2	a	s
	6	1	1/2	s	a
$^4P_{1/2}$	7	1	3/2	m_1	$-m_2$
	8	1	3/2	m_2	m_1
	9	1	3/2	m_1	$-m_2$
	10	1	3/2	m_2	m_1
$^4D_{1/2}$	11	2	3/2	m_1	$-m_2$
	12	2	3/2	m_2	m_1
	13	2	3/2	s	a
	14	2	3/2	a	s
	15	2	3/2	m_1	$-m_2$
	16	2	3/2	m_2	m_1

2A). Not all of the 16 states shown in Table I are equally important and in the central and tensor calculation the symmetric S state and all the P states are omitted altogether, (i.e., state 2 and states 5 to 10), thereby reducing the overall computing time by about a factor of three. The arguments of [3, p. 501] as well as the calculations of [3, p. 505] suggest that this omission has only a small effect on the eigenvalue. However our reason for omitting these states was to provide a trial problem of intermediate complexity which can be solved unambiguously and accurately. As a result of this omission there are nine remaining states in the expansion of the ground state wave function:

$$\Psi = \Phi \sum_{l=1}^{9} f_l(r_{23}, r_{31}, r_{12})\, Y_l \qquad \text{(Euler angles, spin, isospin)}, \tag{3}$$

where Φ is a function of the center of mass coordinates and where l is redefined so

that $l = 1, 2,..., 9$ includes states 1, 3, 4, 11–16 of Table I. In this expansion the six remaining coordinates after separation of center of mass coordinates are taken to be three interparticle distances r_{23}, r_{31}, and r_{12} and three Euler angle coordinates defining the orientation of the triangle in space. This expansion separates the known dependence of the wavefunction on the spin, isospin, and Euler angles from the unknown dependence on the interparticle distances. (The Y_l representing the regular and nonorthogonal D states also have a certain prescribed dependence on interparticle distances not indicated in (3).) By substituting (3) into (1), integrating over angles, and summing over spins and isospins, a set of nine linked partial-differential equations in three interparticle distances is obtained in the form

$$H\psi = E\rho N\psi. \tag{4}$$

For the present calculation this equation has been transformed to three new variables u_1, u_2, and u_3 (Section 2A) defining the unit cube of Fig. 1. The wave-

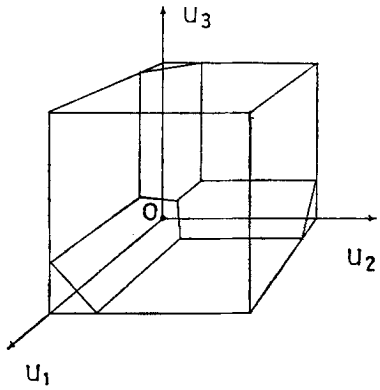

FIG. 1. Unit cube configuration space of the triton problem in u coordinates. The origin 0 corresponds to coincidence of the three particles. The skirting boards are the plane surfaces of the hard core region.

function ψ is a nine component vector whose elements f_l, $l = 1, 2,..., 9$, are the expansion coefficients of the ground state, and are functions of the u_r, $r = 1, 2, 3$. The permutation symmetry of the f_l is conjugate to that of the Y_l so that the ground state Ψ is antisymmetric in agreement with Pauli's principle. H, the hamiltonian, is a 9×9 real hermitian matrix acting on the f_l whose elements consist of functions of the u_r as well as linear differential operators of first and second order (Section 2). ρ is a positive definite function of the u_r and N a positive semidefinite symmetric matrix whose matrix elements are functions of the u_r. (N is a normalization matrix that is present because of the choice of the regular and nonorthogonal

set of D states.) In the S state problem, (4) simplifies to a single equation of the form

$$H\psi = \left[-\hbar^2/2M \sum_{r,s=1}^{3} \frac{\partial}{\partial u_r}\left(\rho g_{rs} \frac{\partial}{\partial u_s}\right) + \rho \sum_{r<s} V_{rs}\right]\psi = E\rho\psi, \tag{5}$$

where the g_{rs} are functions of the u_r defined in Appendix A and the V_{rs} are functions of the u_r defined in [17].

B. *The Numerical Approach*

A direct numerical approach is used to solve equations (4) and (5). A simple cubic lattice of mesh points is introduced into the unit cube of u space thereby preserving the symmetry with respect to permutations of particles. Functions of three variables are represented by three-dimensional tables of numbers. The choice of finite-difference operators replacing derivatives is made so that the resulting finite-difference matrix is transpose–symmetric (this symmetry being the numerical analog of the hermitian symmetry of the analytic operator) and so that differentiation is validly represented near the boundaries of the cube. It did not seem possible to meet these requirements, which were felt to be important for successful extrapolation (Section 1C), with other than first-order finite-difference operators. (Nevertheless, Winter and McKoy [26] seem to obtain successful extrapolation using higher-order finite-difference operators that do not preserve hermitian symmetry). Integration is represented by the Riemann sum including a factor h^3 for the volume element, where h is the mesh size. The eigenvalue–eigenfunction problem (4) is thus replaced by the eigenvalue–eigenvector problem

$$H\psi = \lambda\rho N\psi, \tag{6}$$

where the nine component eigenvector ψ consists of nine tables of numbers representing the f_i and where H and ρN are finite matrices. The choice of the transformation function defining the independent variables u_r is made so that even on a coarse mesh the overall shapes of the f_i are effectively seen. In this respect and also in respect of the preservation of rotational, permutation, and hermitian symmetries, (6) is expected to be a good numerical model of the analytical problem. Equation (6) is solved iteratively on a sequence of meshes of decreasing size for the fundamental eigenvalue $\lambda = \lambda(h)$ and corresponding eigenvector. The sequence of eigenvalues is obtained to high accuracy so as to provide a firm basis for high-order extrapolation to the limit of zero mesh size.

Several authors have applied finite-difference techniques to Schrödinger's equation for various systems obtaining the problem in the form of an eigenvalue–eigenvector problem [11, 26]. In the three nucleon problem finite-difference techniques have been used by Laverne and Gignoux [11] who reduce the problem

TABLE II

Eigenvalues λ as a Function of Mesh Size h for the Central and Tensor problem, Eqs. (4) and (6), with Table of Extrapolations of λ to $h=0$, Indicating Convergence to a Limit Between 4 and 5 MeV

h	λ (MeV)					
1/15	18.28227					
		−0.18041				
1/20	13.66660		4.90219			
		1.85262		4.13373		
1/25	11.30380		4.51796		4.38826	
		2.74107		4.27918		
1/30	9.87668		4.41563			
		3.21951				
1/35	8.92566					

TABLE III

Eigenvalues λ as a Function of Mesh Size h for the S State Problem, Eq. (5), with Table of Extrapolations of λ to $h = 0$, Converging on about 7.8326 MeV

h	λ (MeV)						
1/16	18.46748395						
		4.8378665					
1/24	13.92427815		8.2655370				
		6.5517018		7.779243			
1/32	12.08113405		7.9737610		7.83879		
		7.1205255		7.818944		7.83248	
1/40	11.08901233		7.8963528		7.83429		7.83261
		7.3791346		7.827711		7.83258	
1/48	10.47069937		7.8669349		7.83322		
		7.5185061		7.830464			
1/56	10.04895747		7.8532586				
		7.6021942					
1/64	9.743112067						

TABLE IV

Eigenvalues λ as a Function of Mesh Size h for the Deuteron with *HJ* Potential, with Table of Extrapolations of λ to $h = 0$, Converging on about 2.269 MeV[a]

h	λ (MeV)					
1/16	6.094754215					
		1.56272643				
1/32	3.828740326		2.2858115			
		2.04478315		2.276299		
1/48	3.234087935		2.2786775		2.26824	
		2.16173036		2.269856		2.26903
1/64	2.965998542		2.2733849		2.26890	
		2.20639220		2.269223		
1/80	2.814077275		2.2713040			
		2.22802949				
1/96	2.716402645					

[a] The numerical problem is a finite-difference representation of Schrödinger's equation which reduces to a pair of coupled differential equations [40].

TABLE V

Eigenvalues λ as a Function of Mesh Size h for the Two Particle Exponential Well Problem with Hard Core, with Table of Extrapolations of λ to $h = 0$ Converging on about 8.44495 MeV[a]

h	λ (MeV)						
1/16	10.36664066						
		8.29773807					
1/24	9.67700646		8.44265957				
		8.37019882		8.4445085			
1/32	9.35030455		8.44376895		8.4450312		
		8.39962687		8.4448570		8.444972	
1/40	9.16016902		8.44431300		8.4449890		8.444954
		8.41452225		8.4449324		8.444958	
1/48	9.03589456		8.44457849		8.4449697		
		8.42310975		8.4449511			
1/56	8.94835387		8.44471823				
		8.42851187					
1/64	8.88337362						

[a] The numerical problem represents Schrödinger's equation, which reduces to an ordinary differential equation [40].

to a finite set of coupled two-dimensional partial integro-differential equations by making a partial wave expansion of the Faddeev equations in configuration space and by omitting all two nucleon angular momentum states except for a few low lying states in which the nucleon–nucleon interaction is known to be significant. This truncation introduces a kind of ambiguity into their calculation which is absent from ours. Their numerical approach to the equations using inverse iteration (Section 1E) and successive overrelaxation (Section 1F) is similar to our approach but seems to be less sophisticated. The quoted numerical accuracy of their result (about three figures) lacks supporting evidence such as the extrapolation table which we provide.

The direct application of finite-difference techniques to Schrödinger's equation for the three nucleon problem as described in this paper seems to be new.

C. *The Results*

The binding energy results for the two and three particle problems are shown in Tables II to V. The first columns of the tables contain the eigenvalues $\lambda(h)$. Successive columns are generated by eliminating successive powers of h from the error $\lambda(h) - \lambda(0)$, assuming that $\lambda(h)$ may be expanded in a power series in h (Section 4A). Thus in column two the leading (linear) term in the error is eliminated and in column three the quadratic term, and so on. The lowest line of a table contains the most accurate estimates of the analytic eigenvalue since these pertain to the finest mesh sizes, and among these the accuracy increases in traveling from left to right across the tables. In the S state and deuteron problems the convergence is very rapid resulting in binding energies of 7.8326 MeV [17], 8.44496 MeV, and 2.269 MeV [17], respectively, with five, six, and four figures accuracy. These results may be compared, respectively, with 7.96 ± 0.14 MeV [27] and 7.82 MeV [28] found variationally, 8.44496 MeV [29] found analytically, and 2.269 MeV [4]. In the central and tensor problem the binding energy, between 4 and 5 MeV [18], has only about one figure accuracy. This result is sufficiently accurate to indicate a discrepancy with Chi-yu Hu's variational result of 2.8 MeV [16], and its accuracy could be improved, at the expense of extra computing time, by calculating finer mesh eigenvalues.

The technique of extrapolation using Padé approximations [41] was tried out but found to offer no improvement in accuracy.

D. *Testing the Analysis*

The complexity of the problem makes it essential to test for algebraic errors and errors of transcription made in setting up the numerical representation and in writing the program. A searching test of the numerical analysis and also, indirectly,

of the analysis of Derrick and Blatt was made using a method described fully in [20]. In the test the result of the three nucleon hamiltonian acting on a wavefunction is worked out in two independent ways and compared. An analytic result is obtained directly by substituting into the left-hand side of (1) a three nucleon wavefunction having the quantum numbers appropriate to the ground state and having the product form appropriate to the case where the Hamada–Johnston potential is switched on between only two of the three nucleons. Since, in this case, the hamiltonian operator separates into the sum of a two particle hamiltonian and a free particle hamiltonian, its action on the product wavefunction is easily worked out using Schrödinger's equation for the deuteron [14]. An accurate numerical result can be obtained for comparison by expanding the product wavefunction in terms of the Y_l as in (3), by using the methods of [31] to determine the associated expansion coefficients f_l explicitly, by substituting these f_l into the left-hand side of (6), and by extrapolating the result of this on a sequence of mesh sizes. Individual parts of the hamiltonian, kinetic energy, and central, tensor and spin-orbit potential energy, were tested in this way by setting the other parts to zero. Individual spin and parity terms in the potential were tested by taking the two particle wavefunction in the different spin and parity states. Agreement between analytic and numerical results was obtained to high accuracy in every case. An independent and direct test of the transpose symmetry of H was made by comparing the scalar product of ψ_1 and $H\psi_2$ with the scalar product of ψ_2 and $H\psi_1$ for various choices of ψ_1 and ψ_2; and of the permutation symmetry by comparing the expectation

E. *Inverse Iteration*

The basic method used for solving (6) is "inverse iteration," that is

$$(H - \lambda' \rho N)\, \psi_{n+1} = \rho N \psi_n \,, \tag{7}$$

where λ' is an approximation to the fundamental eigenvalue $\lambda = \lambda(h)$ and ψ_n is an approximation to the corresponding eigenvector. An improved approximation to λ is then given by the Rayleigh quotient

$$\frac{\psi_{n+1}^T H \psi_{n+1}}{\psi_{n+1}^T \rho N \psi_{n+1}} = \lambda_{n+1} \,, \tag{8}$$

in which the symmetry of H and ρN guarantees that λ_{n+1} is an upper bound on λ and approximates λ with an error that is quadratic in the error in ψ_{n+1}. If λ' is sufficiently close to λ then λ_n converges to λ and if λ' is set equal to λ_n in (7) then the convergence is very rapid, the number of significant figures trebling at each iteration [32].

F. *Successive Overrelaxation*

The representation of the numerical problem is restricted to internal mesh points outside the hard core (Fig. 1). The permutation symmetry of the problem is used to further restrict the problem to mesh points within one of the six tetrahedra making up the cube. The number of inhomogeneous equations represented by (7) is accordingly about equal to $9 \times (M-1)^3/6$, where $M = h^{-1}$. These equations are solved iteratively by successive overrelaxation by lines [33]. Successive overrelaxation by lines for the symmetric matrix $H - \lambda' \rho N$ converges if the matrix is positive definite, i.e., if λ' is taken less than the fundamental eigenvalue λ (Section 5A). The coefficient data connected with the solution of these equations is reduced by about a half by using the transpose symmetry of H. The detailed logic involved in programming the permutation and transpose symmetry reductions of the numerical problem was tested directly using a relation based on the defining equations of successive overrelaxation (Section 5A).

G. *Combining Inverse Iteration and Successive Overrelaxation*

The overall scheme thus involves two levels of iteration: an outer level of inverse iteration and an inner level of successive overrelaxation. Tables VI and VII illustrate

TABLE VI

Information and Output Connected with Computations on $h = \frac{1}{24}$ in the S State Problem (Table III) Indicating Convergence of Successive Outer Iterations[a]

n	k_n	RHS	λ'(RHS$\neq$0) or λ_{n-1}(RHS=0)	λ_n	Q_n	$R_n^2/110^b$	$\lambda_n - \lambda_5$	$r_a{}^c$
0	0	—	—	−11.81	−24.02	0.40(1)[e]	0.21(1)	—
1	13	$\neq$0	−15.223	−13.493	−16.681	0.90(0)	0.43(0)	—
2	32	$\neq$0	−15.223	−13.9082	−13.9832	0.18(−1)	0.16(−1)	—
3	21	0	λ_2	−13.92305	−13.92879	0.13(−2)	0.12(−2)	—
4	17	0	λ_3	−13.92427645	−13.9242832	0.17(−5)	0.17(−5)	1/30
5	35	0	λ_4	−13.924278152[d]	−13.924278154	0.40(−9)	0.0	1/15

[a] Both the nonzero RHS procedure, Eqs. (7) (see footnote *f*), (8), and (12), and the zero RHS procedure, Eqs. (9), (8) and (13) are used.

[b] R_n^2 is normalized to agree with $\lambda_n - \lambda_5$ at $n = 4$.

[c] r_a gives the reduction in the SOR difference vector norm following a successful application of the acceleration device (43), where r_a is the subsequent SOR ratio (42) (e.g., $r_a = r^{(91)}$ in Table XII).

[d] The eigenvector corresponding to λ_5 is shown in Fig. 5.

[e] Bracketed numbers are exponents of 10.

[f] In the S state problem in Eq. (7) etc. $N = 1$.

TABLE VII

Information and Output Connected with Computations on $h = \frac{1}{30}$ and $h = \frac{1}{35}$ in the Central and Tensor Problem (Table II) Indicating Convergence of Successive Outer Iterations[a]

n	k_n	RHS	λ' or λ_{n-1}	λ_n	Q_n	$R_n^2/65$[b]	$\lambda_n - \lambda_8$[b]	r_a
				Mesh size $h = \frac{1}{30}$				
0	0	—	—	−4.10	−77.06	0.90(2)	0.57(1)	—
1	14	≠0	−10	−9.19	−13.58	0.15(1)	0.68(0)	—
2	15	≠0	−10	−9.73	−20.42[d]	0.50(1)[d]	0.14(0)	2/5
3	11	≠0	−15	−9.844	−10.406	0.18(0)	0.33(−1)	—
4	9	≠0	−11	−9.856	−9.966	0.34(−1)	0.20(−1)	—
5	34	≠0	−11	−9.87625	−9.87798	0.50(−3)	0.43(−3)	1/8
6	39	0	−9.878	−9.876648	−9.876758	0.34(−4)	0.34(−4)	1/2
7	37	0	λ_6	−9.8766810	−9.8766885	0.23(−5)	0.12(−5)	—
8	17	0	λ_7	−9.8766822[c]	−9.8766870	0.14(−5)	0.0	—
				Mesh size $h = \frac{1}{35}$				
0	0	—	—	−8.70	−50.03	0.38(2)	0.22(0)	—
1	65	≠0	−9.00	−8.9199	−8.9375	0.48(−2)	0.57(−2)	1/5
2	92	0	−8.93	−8.925569	−8.925918	0.97(−4)	0.97(−4)	1/4
3	124	0	−8.9259	−8.925666	−8.925670	0.83(−6)	0	1/6

[a] Using zero and nonzero RHS procedures.

[b] R_n^2 is normalized to agree with $\lambda_n - \lambda_8$ at $n = 6$ rather than at $n = 7$, the accuracy of $\lambda_7 - \lambda_8$ being in doubt. For $h = \frac{1}{35}$ replace headings by $R_n^2/63$ and $\lambda_n - \lambda_3$.

[c] The symmetric S and D components of the eigenvector corresponding to λ_8 are shown in Figs. 3 and 4.

[d] The anomalous increase in R_2 and $|Q_2|$ seems to indicate that here the acceleration device produces an error vector $\psi_2 - \psi$ with reduced norm but with enhanced weight in R_2 and Q_2.

the combining of these two levels in both the S state and central and tensor calculations. The nth outer iteration is composed of a cycle of k_n inner iterations generating approximate eigenvectors $\psi_n^{(k)}$. The convergence of the overall process depends on the separation between the eigenvalue estimate λ' and the fundamental eigenvalue λ, a narrow separation favoring inverse iteration and a wide separation favoring successive overrelaxation. It was found expedient to take λ' as close to λ as possible, in which case successive overrelaxation was found to converge slowly though smoothly. This permitted the use of an acceleration device which worked very well in the S state problem and reasonably well in the central and tensor problem (Section 5B). As soon as the Rayleigh quotient λ_n becomes sufficiently accurate it speeds up the convergence to replace λ' by λ_n and use the "zero right-hand side" procedure, abbreviated "zero RHS," (Section 5C), defined by the homogeneous equations

$$(H - \lambda_n \rho N)\,\psi_{n+1} = 0, \tag{9}$$

replacing the "nonzero RHS" procedure, Eq. (7). Although $H - \lambda_n \rho N$ is not positive definite since $\lambda_n > \lambda$, nevertheless successive overrelaxation initially converges in this case provided the matrix is sufficiently singular, that is provided the error in λ_n is in some sense smaller than the error in ψ_{n+1}. When these two errors become comparable convergence ceases and this is used to provide a natural indicator of when to terminate an inner cycle of iterations. The outer iterations are terminated as soon as the root mean square residual

$$R_n = \left[\frac{\psi_n{}^T(H - \lambda_n \rho N)\,\rho^{-1}N^{-1}(H - \lambda_n \rho N)\,\psi_n}{\psi_n{}^T \rho N \psi_n}\right]^{1/2}, \tag{10}$$

becomes sufficiently small. The proportionality between $R_n{}^2$ and the error in λ_n expected on theoretical grounds was found to hold in practice (as, for example, in Tables VI and VII), thereby confirming the accuracy of the eigenvalues quoted in the first columns of Tables II–V. An additional guide to the accuracy of the eigenvalues is provided by the quantity

$$Q_n = -\left[\frac{\psi_n{}^T H \rho^{-1} N^{-1} H \psi_n}{\psi_n{}^T \rho N \psi_n}\right]^{1/2}, \tag{11}$$

which appears in practice to function as a lower bound on λ. Although Q_n can only be proven to be less than λ_n and not necessarily less than λ (this follows from expanding the inequality $R_n{}^2 > 0$) nevertheless, in cases where the convergence was not too slow, Q_n often provided a lower bound on λ of high accuracy (as, for example, in Tables VI and VII where the inequality $\lambda_n > \lambda > Q_n$ is obeyed for each n with λ_n and Q_n having comparable accuracy). That in practice Q_n tends in the limit to a lower bound on λ seems to indicate that the process quickly damps out any eigenvector components of the error $\psi_n - \psi$ corresponding to eigenvalues in the positive spectrum of H that are closer to zero than λ (the absence of which eigenvalues would make Q_n a strict lower bound). The iterations are started ($n = 0$) with eigenvalue estimates λ' obtained on coarse meshes by experimenting and on fine meshes by extrapolation (Section 4B) and with eigenvector estimates obtained on coarse meshes by representing variational solutions [19, 37] and on fine meshes by extrapolation (Section 4B). An extrapolated eigenvector is obtained from a sequence of coarse mesh eigenvectors by first interpolating (in three dimensions) approximations to the fine mesh eigenvector and then extrapolating. Starting vectors ($k = 0$) for the cycle of inner iterations belonging to the $(n + 1)$th outer iteration are given by

$$\psi_{n+1}^{(0)} = \frac{\psi_n}{\lambda_n - \lambda'}, \tag{12}$$

in the nonzero RHS scheme, and by

$$\psi_{n+1}^{(0)} = \psi_n, \tag{13}$$

in the zero RHS scheme, where ψ_n abbreviates $\psi_n^{(k_n)}$. (That $\psi_{n+1}^{(0)}$, Eq. (12), approximates ψ_{n+1} when ψ_n approximates ψ follows from (7) by replacing ψ_{n+1} by $\psi_{n+1}^{(0)}$).

2. The Analytic Problems

This section gives detailed descriptions of Eqs. (4) and (5).

A. *The Introduction of u Coordinates*

The choice of u coordinates replacing interparticle distances facilitates the numerical representation of the problem in that it simplifies the geometry of configuration space and eliminates the need for a cut-off in the integrations. The region of configuration space over which the interparticle distances are free to vary has rather awkward boundaries defined by the triangle conditions $-r_{23} + r_{31} + r_{12} \geqslant 0$, etc. By transforming to coordinates similar to those used by Pekeris [34],

$$x_1 = -r_{23} + r_{31} + r_{12},$$
$$x_2 = r_{23} - r_{31} + r_{12},$$
$$x_3 = r_{23} + r_{31} - r_{12},$$

configuration space becomes an infinite cube, the triangle conditions implying that $0 \leqslant x_r \leqslant \infty$, $r = 1, 2, 3$. This infinite cube is reduced to the unit cube of Fig. 1 by means of a further transformation $x_r = \phi(u_r)$, where $0 \leqslant u_r \leqslant 1$ and where the "squeezing function" ϕ, defined in Section 4A, is a function of u increasing monotonically from 0 to ∞.

The numerical representation takes into account the behavior of the wavefunction in the following special regions of configuration space.

1. When one or more of the interparticle distances tends to infinity the bound state wavefunction tends to zero. This "infinity" region is represented in the cube by the three faces $u_r = 1$ passing through (1, 1, 1). On these three faces $f_l = 0$, $l = 1, 2, \ldots, 9$.

2. When one or more of the interparticle distances is less than or equal to c, the hard core radius, the wavefunction vanishes. This "hard core" region is represented in the cube by the region containing the origin and bounded by the "skirting boards" $x_2 + x_3 = 2c$, etc. and here $f_l = 0$, $l = 1, 2, \ldots, 9$. The skirting board geometry is preserved in u coordinates by taking ϕ linear between $u_r = 0$ and $u_r = \phi^{-1}(2c)$.

3. When the three particles are in line, e.g., $r_{23} = r_{31} + r_{12}$, or when the three particles form an equilateral triangle $r_{23} = r_{31} = r_{12}$ then the Euler angles are not uniquely defined and the wavefunction obeys certain asymptotic conditions.

(If it did not, a neighborhood of these configurations would make an infinite positive contribution to the expectation value of the kinetic energy operator.) The first region is represented by the three "in-line" faces of the cube $u_r = 0$ passing through the origin, where some of the f_l tend to a constant as u_r tends to zero. The second region is represented by the principal diagonal of the cube and here, as a result of using Derrick's regular D state functions referred to in Section 1A, the special asymptotic conditions are incorporated into these functions and the f_l are simply regular.

B. *The Kinetic Energy Operator*

Derrick [23, 24] has obtained the operator $(\nabla_1^2 + \nabla_2^2 + \nabla_3^2)$ in (1) in the form of a 16×16 matrix of operators which in the nine state central and tensor problem reduces to a 9×9 matrix

$$T = \begin{bmatrix} K & \cdot & \cdot & & & & & & \\ \cdot & K & \cdot & & & & & & \\ \cdot & \cdot & K & & & & & & \\ & & & K_0 & \cdot & K_1+M_1 & -K_2-M_2 & K_1+M_1 & -K_2-M_2 \\ & & & \cdot & K_0 & K_2+M_2 & K_1+M_1 & -K_2-M_2 & -K_1-M_1 \\ & & & K_1-M_1 & K_2-M_2 & K_5 & L & -K_3 & -K_4 \\ & & & -K_2+M_2 & K_1-M_1 & -L & K_5 & -K_4 & K_3 \\ & & & K_1-M_1 & -K_2+M_2 & -K_3 & -K_4 & K_5 & L \\ & & & -K_2+M_2 & -K_1+M_1 & -K_4 & K_3 & -L & K_5 \end{bmatrix}, \tag{14}$$

acting on the nine components f_l, where

$$\begin{aligned} K &= \sum_{r,s=1}^{3} (\partial/\partial u_r)(\rho g_{rs}(\partial/\partial u_s)), \\ L &= \sum_{r=1}^{3} \rho l_r(\partial/\partial u_r), \\ M_1 &= \sum_{r=1}^{3} \rho m_{1r}(\partial/\partial u_r), \\ M_2 &= \sum_{r=1}^{3} \rho m_{2r}(\partial/\partial u_r), \end{aligned} \tag{15}$$

and

$$K_q = \sum_{r,s=1}^{3} (\partial/\partial u_r)(N_q \rho g_{rs}(\partial/\partial u_s)), \qquad q = 0, 1, \ldots, 5.$$

The operators K, K_0, and K_5 are hermitian and symmetric with respect to permutations, (K_1, K_2) and (K_3, K_4) are hermitian and mixed symmetric, L is antihermitian and antisymmetric, and (M_1, M_2) are antihermitian and mixed symmetric. The overall hermitian property of (14) implies that an operator and its hermitian conjugate occur in symmetric positions with respect to the diagonal of the matrix. The overall permutation symmetry of (14) implies that under the permutation operator P_{23}, for example, T transforms as

$$P_{23}T = R_{23}TR_{23}^{-1}, \tag{16}$$

where R_{23} is a 9×9 permutation matrix acting on the f_l and defined by equations similar to (2). The coefficients of derivatives involving the quantities ρ, g_{rs}, l_r, m_{1r}, m_{2r}, and N_q given in Appendix A are functions of the u_r of well-defined permutation symmetry. By virtue of the following property

$$\begin{aligned} g_{rs}(u_r = 0) &= 0, \\ l_r(u_r = 0) &= 0, \\ m_{1r}(u_r = 0) &= 0, \\ m_{2r}(u_r = 0) &= 0, \end{aligned} \tag{17}$$

the coefficients of derivatives vanish on the in-line faces of the cube, an important point for the numerical representation.

C. *The Potential Energy Operator*

The full Hamada–Johnston potential operator [14] may be expressed formally as a finite sum

$$V_{ij} = \sum_{m=1}^{12} V_m O_m . \tag{18}$$

Each term $V_m O_m$ in this sum is associated with one of the four spin and parity states of the two nucleons i and j: triplet-even, triplet-odd, singlet-even, and singlet-odd, and also each term is associated with one of the four types of potential: central, tensor, spin-orbit, and quadratic spin-orbit (thus central triplet-even terms, etc.). The functions V_m of the interparticle distance r_{ij} are positive and infinite within the hard core ($r_{ij} \leqslant c = 0.485345$ fm) outside of which they are steeply peaked monotonic functions tending rapidly to zero. The O_m and hermitian operators commuting with the V_m and act on the spin and isospin coordinates (and

also, in the case of the spin-orbit terms, on the cartesian coordinates as first- and second-order differential operators). In the Derrick–Blatt formalism the O_m are represented by matrices of operators acting on the f_l. For example, the O_m associated with the central triplet-even potential between particles 1 and 2 is given by the symmetric matrix

$$\begin{bmatrix} \frac{1}{2} & \cdot & -\frac{1}{2} & & & & & & \\ \cdot & \cdot & \cdot & & & & & & \\ -\frac{1}{2} & \cdot & \frac{1}{2} & & & & & & \\ & & & \cdot & \cdot & \cdot & \cdot & \cdot & \cdot \\ & & & \cdot & d_0 & d_2 & d_1 & -d_2 & -d_1 \\ & & & \cdot & d_2 & d_4 & d_3 & -d_4 & -d_3 \\ & & & \cdot & d_1 & d_3 & d_5 & -d_3 & -d_5 \\ & & & \cdot & -d_2 & -d_4 & -d_3 & d_4 & d_3 \\ & & & \cdot & -d_1 & -d_3 & -d_5 & d_3 & d_5 \end{bmatrix}.$$

where the d's are functions of the u_r defined in Appendix A.

In (4) the hamiltonian is

$$H = (-\hbar^2/2M)\, T + \rho V_{23} + \rho V_{31} + \rho V_{12}\,, \tag{19}$$

where $\hbar^2/2M = 20.73627$ MeV fm^2. V_{23} and V_{31} are obtained from V_{12} by permutation symmetry. Thus $V_{23} = R_{31} V_{12} R_{31}^{-1}$ and $V_{31} = R_{23} V_{12} R_{23}^{-1}$. The algebra involved in the matrix multiplications is done on the computer.

3. The Finite-Difference Representation

This section describes the numerical representation of Eqs. (4) and (5).

A simple cubic lattice of mesh points is introduced into the unit cube of u space by taking M intervals of equal length $h = M^{-1}$ along each axis thereby preserving permutation symmetry. The mesh point P with indices i, j, k has u coordinates $u_1 = (i-1)\,h$, $u_2 = (j-1)\,h$, $u_3 = (k-1)\,h$ and the complete lattice is generated by giving i, j, k the values $1 \leqslant i, j, k \leqslant M+1$. A function $f(u_1, u_2, u_3)$ is represented by a table of values $f(i, j, k)$.

In the S state problem the operator K, Eqs. (5) and (15), is represented by the finite-difference operator

$$K = \sum_{r,s=1}^{3} (-\Gamma_r)^T \rho g_{rs} \Gamma_s\,. \tag{20}$$

Γ_s is a direct product of a matrix Γ operating on the u_s subspace and unit matrices operating on the u_r subspaces ($r \neq s$), where

$$\Gamma = h^{-1}\begin{bmatrix} -1 & 1 & 0 & 0 & & & \\ 0 & -1 & 1 & 0 & & \cdots & \\ & & -1 & 1 & & & \\ & & & & -1 & 1 & 0 \\ & \cdots & & & 0 & -1 & 1 \\ & & & & 0 & 0 & -1 \end{bmatrix}. \tag{21}$$

The representation of the problem is restricted to internal points of the cube, and indeed to points outside the hard core, within and on which the wavefunction vanishes. The first row of Γ pertains to a point adjacent to an in-line face of the cube and the last row pertains to a point adjacent to an infinity face of the cube. Γ_s is essentially the forwards-difference operator divided by h.

$$\Gamma_s f(u_1, u_2, u_3) = (f(u_s + h) - f)/h, \tag{22}$$

and validly represents to first-order in h the derivative of a function vanishing at $u_s = 1$ (in (22) $f(u_s + h)$ stands for $f(u_1 + h, u_2, u_3)$ if $s = 1$, etc.). $\partial/\partial u_s$ in (5) is therefore validly represented by Γ_s since the bound state wave function vanishes at $u_s = 1$. Similarly $\partial/\partial u_r$ in (5) is validly represented by the backwards-difference operator $-\Gamma_r^T$ at points adjacent to an in-line face since, by virtue of (17), g_{rs} vanishes at $u_r = 0$.

K expands into a finite-difference matrix whose coefficients $K_{PP'}$ linking a mesh point P to its neighbors may be obtained by letting (20) act on a function of three variables. One obtains

$$\begin{aligned} \Gamma_r^T \rho g_{rs} \Gamma_s \psi = &- [\rho g_{rs}\{\psi(u_s + h) - \psi\} - \rho(u_r - h)\, g_{rs}(u_r - h) \\ &\{\psi(u_r - h, u_s + h) - \psi(u_r - h)\}]/h^2, \qquad r \neq s, \\ = &- [\rho g_{ss}\psi(u_s + h) + \rho(u_s - h)\, g_{ss}(u_s - h)\, \psi(u_s - h) \\ &- \{\rho g_{ss} + \rho(u_s - h)\, g_{ss}(u_s - h)\}\, \psi]/h^2, \qquad r = s. \end{aligned} \tag{23}$$

Summing over r and s and replacing $\psi(u_1 + h)$ by $\psi(i + 1, j, k)$ etc. yields thirteen nonzero coefficients $K_{PP'}$ for each row of the matrix. These coefficients are presented in Table VIII. The set of 12 neighboring mesh points P' in $\mathcal{N}(P)$ to which P is coupled is shown in Table VIII.

The symmetry of K under transposition is easily established by taking the transpose of (20) and using $g_{rs} = g_{sr}$, $r \neq s$, which follows from the definition of the g_{rs} in Appendix A. The symmetry of K under permutations is also easily

TABLE VIII

The 13 Finite-Difference Coefficients $K_{PP'}$ [a]

Mesh point P'	Reference number r	Coefficient $K_{PP'}$
$(i+1, j, k)$	1	$-\sum_{r=1}^{3} g_{r1}$
$(i, j+1, k)$	2	$-\sum_{r=1}^{3} g_{r2}$
$(i, j, k+1)$	3	$-\sum_{r=1}^{3} g_{r3}$
$(i-1, j, k)$	4	$-\sum_{r=1}^{3} g_{1r}(i-1, j, k)$
$(i, j-1, k)$	5	$-\sum_{r=1}^{3} g_{2r}(i, j-1, k)$
$(i, j, k-1)$	6	$-\sum_{r=1}^{3} g_{3r}(i, j, k-1)$
$(i, j-1, k+1)$	7	$g_{23}(i, j-1, k)$
$(i, j+1, k-1)$	8	$g_{32}(i, j, k-1)$
$(i-1, j, k+1)$	9	$g_{13}(i-1, j, k)$
$(i+1, j, k-1)$	10	$g_{31}(i, j, k-1)$
$(i-1, j+1, k)$	11	$g_{12}(i-1, j, k)$
$(i+1, j-1, k)$	12	$g_{21}(i, j-1, k)$
(i, j, k)	13	$g_{11}(i-1, j, k) + g_{22}(i, j-1, k) + g_{33}(i, j, k-1) + \sum_{r,s=1}^{3} g_{rs}$

[a] Whereby at a particular mesh point $P(i, j, k)$, the result of the operator K, Eqs. (15) and (20), acting on a function of three variables may be represented by a linear combination of function values at P itself (numbered $r = 13$) and at the points P' (numbered $r = 1, 2, \ldots, 12$) defining the set $\mathcal{N}(P)$ of 12 neighboring points. For ease of presentation, a factor ρ/h^2 has been absorbed into the g_{rs}, defined in Appendix A.

established. For example, applying P_{12} to the first coefficient of Table VIII and using the definitions of the ρ and g_{rs} in Appendix A, one obtains

$$\begin{aligned} P_{12}K(i, j, k: i+1, j, k) &= K(j, i, k: j, i+1, k) \\ &= -\frac{\rho(j, i, k)}{h^2}\left(g_{12}(j, i, k) + g_{22}(j, i, k) + g_{32}(j, i, k)\right) \\ &= -\frac{\rho(i, j, k)}{h^2}\left(g_{21}(i, j, k) + g_{11}(i, j, k) + g_{31}(i, j, k)\right) \\ &= K(i, j, k: i+1, j, k). \end{aligned}$$

The coefficients $K_{PP'}$ vanish when P' lies on an in-line face. For example, if $i = 1$, the coefficient linking $(1, j, k)$ to $(0, j, k)$ in Table VIII is $-1/h^2 \sum_{r=1}^{3} \rho g_{1r}(0, j, k)$ which vanishes because of (17). The complete hamiltonian finite-difference matrix representing H, Eq. (5), is obtained by adding to $-(\hbar^2/2M)K$ a diagonal matrix representing the potential.

In the central and tensor problem the D state operators in T, Eq. (14), are represented similarly. For example, the antihermitian operator L is validly represented by $\frac{1}{2}\sum_{r=1}^{3} \rho l_r \Gamma_r - \frac{1}{2}\sum_{r=1}^{3} \Gamma_r^T \rho l_r$ which is antisymmetric both under transpositions and permutations and which defines a matrix with six nonzero elements per row linking the first six points of Table VIII. The complete finite-difference matrix $H_{lm}(P, P')$, $l, m = 1, 2, \ldots, 9$, representing H in Eq. (19) is built up by selecting the operator in the (l, m)th entry in (14) and substituting the (P')th coefficient belonging to that operator, i.e., substituting $K_{PP'}$ for K, $L_{PP'}$ for L, etc. The central and tensor potentials contain no differential operators and so contribute only to the diagonal blocks $H_{lm}(P, P)$. The resulting matrix is symmetric under transposition

$$H(P, P') = (H(P', P))^T, \tag{24}$$

where $H(P, P')$ is a 9×9 block, and is symmetric under permutations

$$H(RP, RP') = RH(P, P')\, R^{-1}. \tag{25}$$

On the left-hand side of Eq. (25) R is a permutation operator and on the right-hand side R is the corresponding 9×9 permutation matrix defined in Section 2B. Equation (4) is represented at each mesh point P by

$$\sum_{P'} H(P, P')\, \psi(P') = \lambda(h)\, \rho(P)\, N(P)\, \psi(P). \tag{26}$$

where $N(P)$ is the 9×9 normalization matrix [24, Eq. (3)] evaluated at P, and where $\psi(P)$ represents the nine component eigenfunction $\psi = (f_i)$ by nine tables of values $\psi_i(P) = f_i(P)$, $i = 1, 2, \ldots, 9$. Equation (26) need only be solved at internal

mesh points outside the hard core. Points P' on or within the hard core or on the infinity faces do not contribute as $\psi(P')$ vanishes there, and points P' on the in-line faces do not contribute as $H(P,P')$ vanishes there by construction. The internal mesh points are ordered with i varying most rapidly, then j, then k ($2 \leqslant i \leqslant M$ etc). Fixed (j, k) may be said to represent a line of wavefunction values and fixed k a plane.

H and ρN are large sparse matrices. ρN is positive definite and is block diagonal with 9×9 blocks. H is block 13 diagonal: the nine rows of H pertaining to the point $P = (i, j, k)$ include (in general) 13 nonzero 9×9 blocks $H_{PP'}$ coupling P to itself and to the twelve neighboring points P' in (6.6) Table VIII (moving

4. The Extrapolation Technique

This section describes how the extrapolation process works and how initial estimates of the eigenvalue and eigenvector suitable for starting iterations on a given mesh may be obtained by extrapolating solutions already obtained on coarser meshes.

A. *Extrapolating the Eigenvalues to Zero Mesh Size*

Tables II to V containing the eigenvalues and extrapolations to $h = 0$ are referred to as Neville tables [35]. The extrapolation process assumes that an analytic function

$$\lambda(h) = \lambda(0) + \nu_1 h + \nu_2 h^2 + \cdots, \tag{27}$$

exists whose values at the mesh sizes indicated in the tables are the corresponding eigenvalues entered in column one, and whose value $\lambda(0)$ at $h = 0$ is the analytic eigenvalue. A term linear in h associated with nonzero ν_1 must be included in accordance with the fact that the leading term in the truncation error of the representation (20) of the derivative is linear in h. The mesh sizes h actually employed may be expressed as submultiples $h = h_0/p$ of a quantity h_0 as, for example, in Table II where $h_0 = \frac{1}{5}$ and $p = 3, 4, \ldots, 7$.

Successive columns of the tables after the first contain successive extrapolations. An entry $\bar{\lambda}$ in some column is obtained from a pair of neighbouring entries λ' and λ'' in the previous column by applying the extrapolation rule

$$\bar{\lambda} = \left(\frac{\lambda'}{h'} - \frac{\lambda''}{h''}\right) \Big/ \left(\frac{1}{h'} - \frac{1}{h''}\right) \tag{28}$$

where h' and h'' are the mesh sizes of the entries in column one symmetrically placed with respect to $\bar{\lambda}$. The effect of (28) is to eliminate successive terms from the error $\lambda(h) - \lambda(0)$ in successive columns, the linear term (proportional to h) being eliminated from the entries in column two, the quadratic term (proportional to h^2) in column three, and so on. By continued application of (28), $\bar{\lambda}$ may be expressed as a linear combination

$$\bar{\lambda} = \sum_p \beta_p \lambda(h_0/p) \tag{29}$$

of the eigenvalues in column one that are symmetrically placed with respect to it. As one moves from left to right across a particular line of the table (say, the lowest) two factors operate simultaneously: the accuracy of the $\bar{\lambda}$ increase as higher-order terms are eliminated from the truncation error, and the rounding error builds up as the β coefficients increase in magnitude (the largest β coefficient in Table III being about 1000). It is for this reason that the eigenvalues in column one are obtained to such high accuracy so as to provide sufficiently noise free extrapolation.

The tables show an overall pattern of convergence. In traveling down successive columns the monotonic convergence of successive approximations, alternating between convergence from above and convergence from below, is evident in Tables II and III. These properties are not always found and in Tables IV and V the alternating property does not hold. The convergence can be spoiled if eigenvalues from too coarse a mesh are included. For this reason the eigenvalues for $h = \frac{1}{5}(111.7946)$ and $h = \frac{1}{10}(30.74207)$ were excluded from Table II, and the eigenvalue for $h = \frac{1}{8}$ (43.59821719) from Table III.

The successful working of the extrapolation process depends on how well the analytic problem has been represented. As a guide to this we studied the overall shapes of ψ and $\psi^T \rho N \psi$ which depend on the choice of the squeezing function ϕ. In the central and tensor problem ϕ was taken to be the two piece function

$$\begin{aligned} \phi(u) &= \frac{2c}{\gamma} u, \qquad 0 \leqslant u \leqslant \gamma, \\ &= \frac{2c}{\gamma} u + \delta \frac{(u-\gamma)^3}{1-u}, \qquad \gamma < u \leqslant 1, \end{aligned} \tag{30}$$

shown in Fig. 2. The c is the hard core radius; ϕ together with its first and second derivatives is continuous; and the linear piece is used so as to preserve the plane "skirting board" geometry of the hard core region indicated in Fig. 1. There is some flexibility built into ϕ in the free parameters γ and δ. Suitable values for γ and δ may be chosen by computing the solution on a coarse mesh and adjusting γ and δ so that the significant features of ψ and $\psi^T \rho N \psi$ are effectively seen on the coarsest mesh employed in the extrapolation and are also reasonably evenly distributed

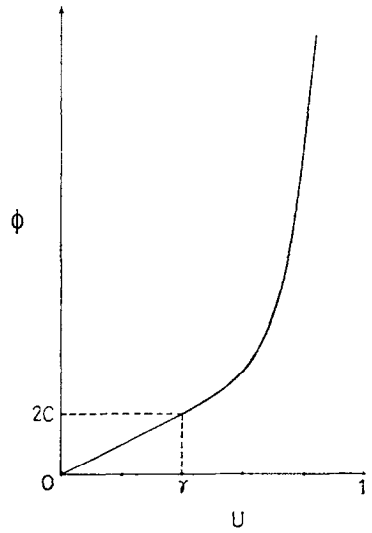

FIG. 2. The two-piece squeezing function ϕ, Eq. (30), used in the central and tensor problem plotted at intervals of the coarsest mesh size $h = \frac{1}{5}$.

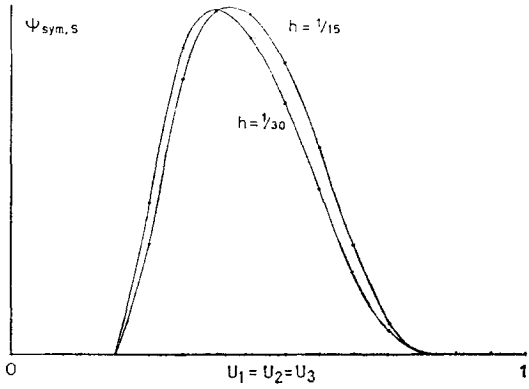

FIG. 3. Values of the symmetric S component (f_1 in Table I) of the eigenvector in the central and tensor problem pertaining to mesh sizes $h = \frac{1}{15}$ and $h = \frac{1}{30}$ and plotted against distance along the principal diagonal of the cube $u_1 = u_2 = u_3$ (where, for the sake of clarity, only values at mesh points whose coordinates are even multiples of h are plotted). The curves are normalized to agree at (6/15, 6/15, 6/15). The main features of the wavefunction in this configuration including the rise from the hard core at (3/15, 3/15, 3/15) to a peak at about (6/15, 6/15, 6/15) and the falloff near (1, 1, 1) seem to be well represented and to be almost independent of mesh size.

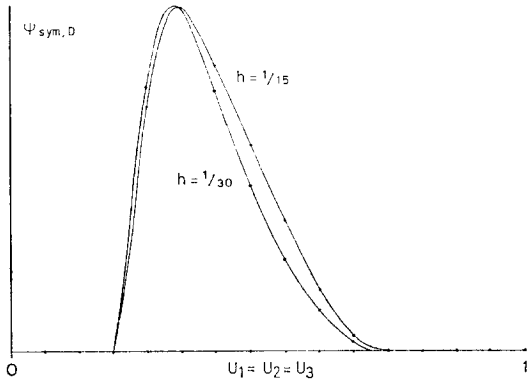

FIG. 4. Values of the symmetric D component (f_{14} in Table I) of the eigenvector in the central and tensor problem pertaining to $h = \frac{1}{15}$ and $h = \frac{1}{30}$ and plotted as in Fig. 3 (with the two curves normalized to agree at (6/15, 6/15, 6/15)). Compared with the S component of Fig. 3 the D component is seen to be more steeply peaked and also to be closer to the hard core.

over u space. These features include the rise along the principal diagonal of the cube from zero at the intersection of the hard core boundaries at $(\frac{1}{2}\gamma, \frac{1}{2}\gamma, \frac{1}{2}\gamma)$ to a peak at about (γ, γ, γ) and the tailing off near (1, 1, 1). These features are clear in the graphs of ψ shown in Figs. 3 and 4. γ was taken to be an even multiple of the quantity $h_0 = \frac{1}{5}$ thus ensuring that a mesh point occurs at $(\frac{1}{2}\gamma, \frac{1}{2}\gamma, \frac{1}{2}\gamma)$ on all meshes. Of the two alternatives, $\gamma = \frac{2}{5}$ or $\gamma = \frac{4}{5}$, the latter was ruled out on the grounds that it gives too much attention to the hard core region and not enough to the infinity region corresponding to a wide separation of the particles. With γ fixed, δ can be thought of as a cut off in configuration space which increases as $1/h$ with

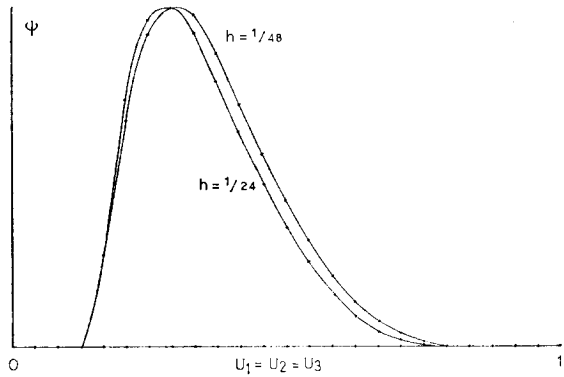

FIG. 5. Values of the symmetric S eigenvector in the S state problem pertaining to mesh sizes $h = \frac{1}{24}$ and $h = \frac{1}{48}$ and plotted against distance along the principal diagonal of the cube.

decreasing mesh size. The choice $\delta = 10$ makes the tailing off of $\psi^T \rho N \psi$ near (1, 1, 1) clearly visible in Fig. 6(i).

Figure 5 shows graphs of solutions to the S state problem and indicates that the various features of the wavefunction have been adequately represented. The nonlinear part of the squeezing function used in the S state problem differed from (30) in having a tail proportional to $u/(1 - u)$ which joined smoothly onto the linear

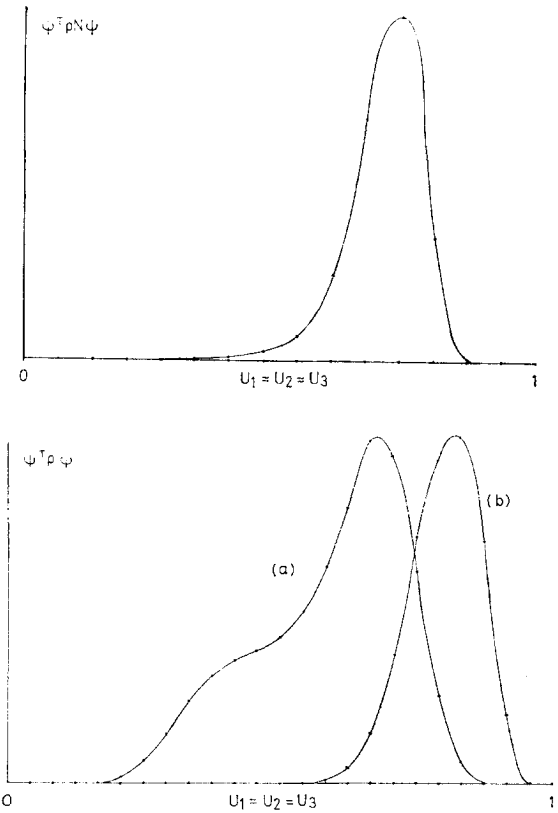

FIG. 6. (i) Values of $\psi^T \rho N \psi$ in the central and tensor problem on $h = \frac{1}{30}$ and (ii) values of $\psi^T \rho \psi$ in the S state problem on $h = \frac{1}{48}$ plotted against distance along the principal diagonal of the cube (and, for the sake of clarity, only at even multiples of mesh size). These curves give some indication of whether or not the particular squeezing function employed in the calculation adequately represents the fall off of ψ near infinity at (1, 1, 1), on which the success of the extrapolation seems to depend (Section 4A). In (i), using the two-piece squeezing function (30), the choice $(\gamma, \delta) = (\frac{2}{5}, 10)$ seems adequate (Figs. 3 and 4 and Table II). In (ii), using a three-piece squeezing function with a linear piece $(2c/\gamma)\, u$ and with a tail-piece $u/(\epsilon(1 - u))$ the choice $(\gamma, \epsilon) = (\frac{1}{4}, 0.7)$ in curve (a) is seen to be adequate (Fig. 5 and Table III); but in curve (b) the choice $(\gamma, \epsilon) = (\frac{1}{2}, 1.6)$ is definitely not adequate and leads to poor extrapolation (Table IX).

piece via a fifth degree polynomial. To illustrate the sensitivity of the extrapolation process to the choice of squeezing function we present in Table IX (to be compared with Table III) results obtained in the S state problem using a squeezing function in which the choice of parameters gave too much attention to the hard core. In traveling from left to right along the lowest line of Table IX the differences between

TABLE IX

An Extrapolation Table for the S State Problem Resulting from Calculations Using a poorer Squeezing Function than that used in Table III (see Section 4A)[a]

h	λ (MeV)						
1/8	18.2223751						
		4.2276864					
1/16	11.2250307		7.624728				
		6.4923809		8.087318			
1/24	9.6474808		7.971671		7.84301		
		7.2320260		7.891875		7.62857	
1/32	9.0436171		7.923793		7.66431		8.02603
		7.5087329		7.740166		7.96925	
1/40	8.7366402		7.831980		7.88212		
		7.6164820		7.821288			
1/48	8.5499472		7.827397				
		7.6767436					
1/56	8.4252038						

[a] The failure of convergence in this case is indicated by the differences of successive entries in the lowest line of the table which are found to eventually increase as one moves from left to right.

successive entries at first decrease but then increase, in contrast with those of Table III which are monotonic decreasing. The poorer squeezing function does not adequately represent the fall off of $\psi^T \rho \psi$ near infinity as is shown in Fig. 6(ii).

The various states in the nine-state central and tensor problem peak in different regions of configuration space. In addition, the mixed and antisymmetric functions are forced by symmetry to have various nodes. All this puts a greater strain on the representation on a coarse mesh and it might be expected that finer meshes would be needed in this problem than in the S state problem, whereas in fact coarser meshes were used. This may account for the poorer extrapolation found in the central and tensor problem.

B. *Initial Values of Eigenvalues and Eigenvectors by Extrapolation*

From the already existing table of extrapolations of coarser mesh eigenvalues to

$h = 0$. This initial estimate is an extrapolation to $h = h_f$ (rather than to $h = 0$). It is an approximation to the last entry in column one of a new extrapolation table whose lowest line pertains to h_f. Approximations to entries in this line may be generated by working from right to left, using (28) in reverse. To start the reverse process, the entry in this line in the same column as the last entry on the right of the previous line is set equal to that entry. Thus, for example, an extrapolated approximation to $\lambda(1/64)$ ($h_f = 1/64$) in Table III was obtained using the table of extrapolations to $h = 0$ of the eigenvalues $\lambda(\frac{1}{16})$ to $\lambda(\frac{1}{56})$. The result -9.74310 has about five figures correct.

In obtaining an initial estimate of the eigenvector it is assumed that an analytic function

$$\psi(\mathbf{u}, h) = \psi(\mathbf{u}, 0) + h\psi_1(\mathbf{u}) + h^2\psi_2(\mathbf{u}) + \cdots, \tag{31}$$

exists whose values at the mesh points $\mathbf{u} = (u_1, u_2, u_3) = ((i - 1)h, (j - 1)h, (k - 1)h)$ on a particular mesh size h are equal to the values of the appropriately normalized eigenvector belonging to that mesh size. $\psi(\mathbf{u}, 0)$ is the normalized fundamental eigenfunction. The power series expansion for the eigenvector is analogous to that for the eigenvalue, Eq. (27). An approximation to the value $\psi(\mathbf{u}, h_f)$ of a fine mesh eigenvector is obtained by extrapolating to $h = h_f$ the sequence of coarse mesh values $\psi(\mathbf{u}, h)$ corresponding to fixed $\mathbf{u}$ and decreasing h. Table X shows extrapolations (to $h = 0$) in the S state problem at points $\mathbf{u}$ restricted

TABLE X

Extrapolations to $h = 0$ in the S State Problem of Eigenvector Values $\psi(\mathbf{u}, h)$, Eq. (31), at Mesh Points Occurring on the Principal Diagonal of the Cube and Contained Within the Common Subset of Points Belonging to $h = \frac{1}{16}, \frac{1}{32}, \frac{1}{48}$, and $\frac{1}{64}$ [a]

Mesh point	Extrapolated value	Variational value
(3/16, 3/16, 3/16)	0.097	0.085
(4/16, 4/16, 4/16)	0.213	0.210
(5/16, 5/16, 5/16)	0.248	0.248
(6/16, 6/16, 6/16)	0.222	0.222
(7/16, 7/16, 7/16)	0.173	0.178
(8/16, 8/16, 8/16)	0.120	0.129
(9/16, 9/16, 9/16)	0.077	0.085
(10/16, 10/16, 10/16)	0.041	0.046
(11/16, 11/16, 11/16)	0.016	0.018

[a] Values of the variational wave function of [19] at the same points are presented for comparison (the upper bound on the analytic eigenvalue associated with this variational wavefunction, -7.5 MeV, should be compared with the extrapolated eigenvalue found in Table III, -7.8326 MeV). The extrapolated and variational wavefunctions are normalized so as to agree at (5/16, 5/16, 5/16). Beyond (11/16, 11/16, 11/16) the eigenvector, which falls off exponentially, is not sufficiently accurate to warrant extrapolation.

to lying on the principal diagonal of the cube and to belonging to the subset of points common to all meshes (which are taken to be submultiples of $h_0 = \frac{1}{8}$). An approximation to a fine mesh value $\psi(\mathbf{v}, h_f)$, where $\mathbf{v}$ is a fine mesh point lying outside this common subset, may be obtained by first interpolating approximations to $\psi(\mathbf{v}, h)$ on the coarse mesh sizes h, and then extrapolating.

The interpolation operator

$$1 + h \sum_{r=1}^{3} \alpha_r \frac{(\Gamma_r - \Gamma_r^T)}{2} + \frac{h^2}{2} \sum_{r,s=1}^{3} \alpha_r \alpha_s (-\Gamma_r^T)\, \Gamma_s\,, \tag{32}$$

acting on the eigenvector $\psi(\mathbf{u}, h)$ belonging to mesh size h approximates $\psi(\mathbf{v}, h)$ to second order in h. Γ_s is the forwards-difference operator (21). The vector $\boldsymbol{\alpha} h \equiv \mathbf{v} - \mathbf{u}$ linking the fine mesh point $\mathbf{v}$ with a particular neighboring coarse mesh point $\mathbf{u}$ is defined in Fig. 7. $\psi(\mathbf{v}, h)$ is approximated by a linear combination of thirteen

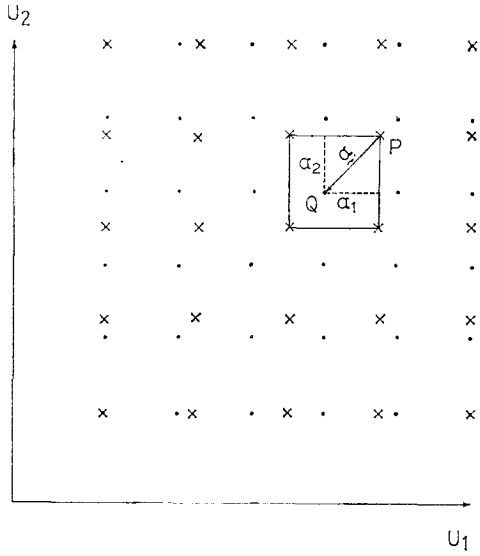

FIG. 7. Fine mesh points with $h_f = \frac{1}{40}$ (dots) and coarse mesh points with $h = \frac{1}{32}$ (crosses) lying on a plane of the cube with $u_3 = \text{const}$ and showing how a point Q in a fine mesh lattice at which an interpolated function value is sought may be related to a point P in a coarser mesh lattice (Section 4B). The vector $\boldsymbol{\alpha}$ in Eq. (32) has, in this example, the value $(-\frac{3}{5}, -\frac{3}{5}, 0)$ (as may be found from $\boldsymbol{\alpha} = (\mathbf{v} - \mathbf{u})/h$ where $\mathbf{v}$ and $\mathbf{u}$ are the position vectors of Q and P). The interpolated function value is expressed as a linear combination of the function values at P and points in $\mathcal{N}(P)$ using the coefficients of Table XI with this particular value of $\boldsymbol{\alpha}$. When Q is adjacent to an in-line face the associated point P is chosen to be adjacent but one so as to avoid references to values at points on the in-line face where the eigenvector is not represented.

neighboring eigenvector values $\psi(\mathbf{u}, h)$, the coefficients of which are defined in Table XI. The similarity of the interpolation operator (32) to the operator K, Eq. (20), helps simplify the programming of the interpolation process, especially at the boundaries of the tetrahedron, where similar procedures are adopted to those described in Appendix B. Equation (32) is a generalization of Newton's

TABLE XI

The 13 Interpolation Coefficients Presented as the Sums of Contributions from Different Powers of the Γ Operators in (32)[a]

Mesh point reference number r	Interpolation coefficients		
	Constant term	Linear terms	Quadratic terms
1		$+\frac{1}{2}\alpha_1$	$+\frac{1}{2}\alpha_1(\alpha_1 + \alpha_2 + \alpha_3)$
2		$+\frac{1}{2}\alpha_2$	$+\frac{1}{2}\alpha_2(\alpha_1 + \alpha_2 + \alpha_3)$
3		$+\frac{1}{2}\alpha_3$	$+\frac{1}{2}\alpha_3(\alpha_1 + \alpha_2 + \alpha_3)$
4		$-\frac{1}{2}\alpha_1$	$+\frac{1}{2}\alpha_1(\alpha_1 + \alpha_2 + \alpha_3)$
5		$-\frac{1}{2}\alpha_2$	$+\frac{1}{2}\alpha_2(\alpha_1 + \alpha_2 + \alpha_3)$
6		$-\frac{1}{2}\alpha_3$	$+\frac{1}{2}\alpha_3(\alpha_1 + \alpha_2 + \alpha_3)$
7			$-\frac{1}{2}\alpha_2\alpha_3$
8			$-\frac{1}{2}\alpha_2\alpha_3$
9			$-\frac{1}{2}\alpha_1\alpha_3$
10			$-\frac{1}{2}\alpha_1\alpha_3$
11			$-\frac{1}{2}\alpha_1\alpha_2$
12			$-\frac{1}{2}\alpha_1\alpha_2$
13	$+1$		$-(\alpha_1^2 + \alpha_2^2 + \alpha_3^2 + \alpha_1\alpha_2 + \alpha_2\alpha_3 + \alpha_3\alpha_1)$

[a] The numbering of points corresponds to that in Table VIII.

interpolation rule [36] to three dimensions. Since the interpolated approximation is correct to only second order in h, it is only permissible to extrapolate a sequence of at most three eigenvectors. Thus, for example, in the S state problem, the eigenvectors belonging to $h = \frac{1}{24}, \frac{1}{32}$, and $\frac{1}{40}$ were extrapolated to $h_f = \frac{1}{48}$ and the approximate eigenvector obtained gave a Rayleigh quotient with three figures correct. In the central and tensor problem, extrapolating from $h = \frac{1}{20}$ and $h = \frac{1}{25}$ to $h_f = \frac{1}{30}$ gave a Rayleigh quotient -9.43 compared with the actual eigenvalue -9.87 (see Table II) and interpolating from $h = \frac{1}{30}$ to $h_f = \frac{1}{35}$ gave a Rayleigh quotient of -8.70 compared with -8.92.

5. Successive Overrelaxation

The method used to solve the inhomogeneous equations (7) in the central and tensor problem and similar equations in the S state problem is successive overrelaxation by lines [33], abbreviated SOR by lines or simply SOR. Because of permutation symmetry the equations need only be solved over one of the six tetrahedra making up the cube, as is described in Appendix B.

A single step of the process consists of updating simultaneously a line of data comprising a number of wavefunction values. In the S state problem a "line" consists of the wavefunction values at mesh points on the (j, k)th line of the cube contained within the basic tetrahedron. In the central and tensor problem a line consists of the nine wavefunction components belonging to a particular mesh point.

A single step of the updating process in the central and tensor problem may be described as follows. The subset of nine equations of (7) pertaining to P may be written in block notation as

$$\sum_{P'} H_{PP'}\psi_{P'} - \lambda'(\rho N)_P\,\psi_P = (\rho N\psi_n)_P\,, \tag{33}$$

where ψ is the latest approximation to ψ_{n+1} in the current SOR cycle, where $H_{PP'}$ is a 9×9 block and $\psi_{P'}$ a nine-rowed column vector, and where the sum over P' includes P as well as the neighboring points $\mathcal{N}(P)$ of Table VIII. At the Pth step of the $(k+1)$th iteration the points P' preceding P in the ordering, $P' < P$, have updated values $\psi_{P'}^{(k+1)}$, whereas P and the points $P' > P$ have values $\psi_{P'}^{(k)}$ not yet updated. The nine components of the vector $\psi_P^{(k+1)}$ updating ψ_P are obtained by solving the nine equations (33) simultaneously for an intermediate result $\psi_P^{(k+(1/2))}$, and then by overcorrecting this result by an amount proportional to the difference $(\psi_P^{(k+(1/2))} - \psi_P^{(k)})$. The equations defining $\psi_P^{(k+1)}$ are

$$\sum_{P'<P} H_{PP'}\psi_{P'}^{(k+1)} + B_P\psi_P^{(k+(1/2))} + \sum_{P'>P} H_{PP'}\psi_{P'}^{(k)} = (\rho N\psi_n)_P\,, \tag{34}$$

and

$$\psi_P^{(k+1)} = \psi_P^{(k)} + \omega(\psi_P^{(k+(1/2))} - \psi_P^{(k)}), \tag{35}$$

where

$$B_P \equiv H_{PP} - \lambda'(\rho N)_P\,, \tag{36}$$

is a 9×9 block, and where the overrelaxation parameter ω satisfies $1 < \omega < 2$. In solving (34) for $\psi_P^{(k+(1/2))}$ all terms not involving $\psi_P^{(k+(1/2))}$ are transferred to the right-hand side which is then left-multiplied by the inverse of B_P. This process, in which the new values $\psi_P^{(k+1)}$ overwrite the old values $\psi_P^{(k)}$, is described as progressive in that each step of the process uses the latest information. The $(k+1)$th iteration,

comprising a number of such individual steps, is completed when all the wave-function values at all the mesh points within the tetrahedron and outside the hard core have been updated.

A. *Convergence of Successive Overrelaxation*

By dividing the matrix $H - \lambda' \rho N$ into its diagonal part $D \equiv (B_p)$ and its upper and lower triangular parts U and L SOR may be described by the equation

$$\psi^{(k+1)} = C\psi^{(k)} + (L + \omega^{-1}D)^{-1} \rho N \psi_n , \tag{37}$$

where the iteration matrix [33]

$$C \equiv 1 - \omega(D + \omega L)^{-1} (H - \lambda' \rho N). \tag{38}$$

Successive difference vectors $d^{(k)} \equiv \psi^{(k)} - \psi^{(k-1)}$ are related by

$$d^{(k)} = Cd^{(k-1)} = \cdots = C^{k-1} d^{(1)}. \tag{39}$$

If the eigenvalue estimate λ' is taken less than λ, the fundamental eigenvalue, then $H - \lambda' \rho N$ is positive definite (as well as being symmetric) and convergence of SOR is guaranteed [33, 39] (with $1 < \omega < 2$; in fact a satisfactory value of $\omega \sim 1.7$ was found experimentally). Under these conditions it follows from (37–39) (see [39, Eqs. (3.56) and (3.57)]) that

$$S^{(k)} \equiv d^{(k)T} (H - \lambda' \rho N) d^{(k)}, \tag{40}$$

is monotonic decreasing, and that the relation

$$S^{(k-1)} - S^{(k)} = ((2/\omega) - 1) \Delta^{(k)T} D \Delta^{(k)}, \tag{41}$$

holds, where $\Delta^{(k)} \equiv d^{(k)} - d^{(k-1)}$ (and where, in the case of SOR reduced to a tetrahedron, the sum over points P implied in the scalar products in (40) and (41) contains a weight factor $w(P)$ defined in Appendix B). In running the program the monotonic property of the $S^{(k)}$ and the agreement of both sides of Eq. (41) were confirmed. This tests that the program reproduces the transpose and permutation symmetries of H, Eqs. (24) and (25), on which (41) depends (in particular, testing the detailed logic needed to reduce the problem to the tetrahedron).

B. *The Acceleration Device*

With λ' only slightly less than λ it is expected that the convergence will be slow since in this case the dominant eigenvalue of C is close to 1 (and, when $\lambda' = \lambda$, is actually equal to 1 as can be seen by applying (38) to the fundamental eigenvector ψ which is now the dominant eigenvector of C). It was found in both the S state and central and tensor problems that although the convergence was indeed extre-

mely slow in this case, it was also quite smooth in the sense that the ratio of successive difference vector norms

$$r^{(k)} \equiv \frac{\| d^{(k)} \|}{\| d^{(k-1)} \|}, \qquad k = 2, 3, \ldots, \tag{42}$$

(defining the norm $\| d^{(k)} \|$ to be the sum of the absolute values of the elements of $d^{(k)}$) eventually settled down to a constant value. When this happened it was found that the simple acceleration device due to Lyusternik [33] in which

$$\frac{\psi^{(k+1)} - r^{(k+1)}\psi^{(k)}}{1 - r^{(k+1)}} \tag{43}$$

k	$\frac{\| d^{(k)} \|}{\| \psi \|_{\max}}$	$r^{(k)}$	$\frac{\| d^{(k)} \|_{\max}}{\| \psi \|_{\max}}$
1	0.367(1)	—	0.198(0)
2	0.276(1)	0.85673884(0)	0.154(0)
3	0.234(1)	0.94706233(0)	0.136(0)
4	0.216(1)	0.10107975(1)	0.121(0)
5	0.197(1)	0.99735135(0)	0.109(0)
.	.	.	.
36	0.508(0)	0.99969552(0)	0.225(−1)
37	0.496(0)	0.99970941(0)	0.220(−1)
38	0.486(0)	0.99970602(0)	0.215(−1)
39	0.475(0)	0.99970153(0)	0.211(−1)
40	0.465(0)	0.99970642(0)	0.206(−1)
.	.	.	.
87	0.234(0)	0.99970509(0)	0.104(−1)
88	0.234(0)	0.99970509(0)	0.103(−1)
89	0.229(0)	0.99970509(0)	0.101(−1)
90	0.227(0)	0.99970509(0)	0.100(−1)
		Acceleration applied	
91	0.405(−10)	0.62565533(−8)	0.409(−11)
92	0.392(−10)	0.96964822(0)	0.486(−11)
93	0.315(−10)	0.80190997(0)	0.253(−11)

[a] The closeness of the limit of the $r^{(k)}$ to 1 is connected with the closeness of the chosen eigenvalue estimate $\lambda' = -21.1$ to the fundamental eigenvalue in this case, $\lambda = -21.04812$.

replaces $\psi^{(k+1)}$, often improved the accuracy. This is illustrated spectacularly (but untypically) in Table XII for a case in which, by direct calculation of the eigenvalues of the iteration matrix C, it was found that the converged ratio was equal to the dominant eigenvalue of C (i.e., 0.99970509) and that the subdominant eigenvalues were all less in magnitude than about 0.7. Under these conditions (39) implies that the subdominant eigenvector components of $d^{(k)}$ will be quickly damped out with the result that the error in $\psi^{(k)}$ consists largely of the dominant component and the effect of (43) is to almost completely eliminate this. The acceleration device seems to work in this way in the examples given in Tables VI and VII where successive applications reduce the estimated total number of iterations by factors of from three to four.

C. *The Zero Right-Hand Side Procedure*

In the zero RHS procedure, Eq. (9), SOR will not ultimately converge since the matrix $H - \lambda_n \rho N$ is not exactly singular [33, p. 240] (the matrix is in fact slightly negative because the upper bound λ_n is necessarily greater than the fundamental eigenvalue λ). However the initial convergence of the process will be unaffected because in

$$\begin{aligned}
\psi_{n+1}^{(k+1)} &= C\psi_{n+1}^{(k)} \\
&= \psi_{n+1}^{(k)} - \omega(D(\lambda_n) + \omega L)^{-1}(H - \lambda_n \rho N)\,\psi_{n+1}^{(k)} \\
&= \psi_{n+1}^{(k)} - \omega(D(\lambda) + \omega L)^{-1}(H - \lambda \rho N)\,\psi_{n+1}^{(k)} \\
&\quad - \omega(D(\lambda_n) + \omega L)^{-1}(\lambda - \lambda_n)\,\rho N \psi_{n+1}^{(k)} \\
&\quad + \omega(D(\lambda) + \omega L)^{-1}(\lambda - \lambda_n)\,\rho N (D(\lambda) + \omega L)^{-1}(H - \lambda \rho N)\,\psi_{n+1+\ldots}^{(k)},
\end{aligned}$$

(using Eq. (38), with $D(\lambda_n)$, $D(\lambda)$ denoting the diagonal parts of $H - \lambda_n \rho N$, $H - \lambda \rho N$, respectively) the terms associated with the departure from singularity, viz, the third, fourth, etc. terms on the right-hand side of the last equation, will be initially too small to be detected. This follows from the quadratic property of the Rayleigh quotient

$$\lambda_n - \lambda \simeq \frac{(\psi_{n+1}^{(0)} - \psi)^T (H - \lambda \rho N)(\psi_{n+1}^{(0)} - \psi)}{\psi^T \rho N \psi},$$

which shows that at $k = 0$ the third term in question is of second order in the error $\psi_{n+1}^{(0)} - \psi$, the fourth term is of third order, etc. and so these terms are negligible in comparison with the first-order second term. When the accuracy of $\psi_{n+1}^{(k)}$ becomes such that the second and third terms are of comparable magnitude the process stops converging. This is indicated during the running of the program

by successive $r^{(k)}$, Eq. (42), becoming greater than one. Therefore this phenomenon provides a natural indicator of when to terminate the current cycle of inner iterations and reevaluate the Rayleigh quotient.

D. *Time and Space Requirements*

The total number of SOR iterations needed to generate solutions of comparable accuracy on different mesh sizes was found to increase gradually with decreasing mesh size, despite the use of better initial approximations on finer meshes obtained by extrapolation (e.g., in the S state problem on $h = \frac{1}{40}$, $\frac{1}{48}$, and $\frac{1}{56}$, about 170, 200, and 220 SOR iterations were needed and in the central and tensor problem on $h = \frac{1}{25}$, $\frac{1}{30}$, and $\frac{1}{35}$ about 170, 180, and 280). The central and peripheral processing times involved were found to increase in somewhat greater proportion than the inverse cube of the mesh size, the total central processing time in the central and tensor calculation amounting to fourteen hours on a CDC CYBER 72. The peripheral processing time, almost completely connected with reading from a CDC 844 disc the coefficient data associated with the $H_{PP'}$ in Eq. (34), was found to be about equal to the central processing time and to be almost concurrent with it. The wavefunction data connected with the $\psi_{P'}$ in Eq. (34) was read sequentially from an input file into an area of central memory where three adjacent planes were stored simultaneously and from which updated data could be written to an output file, the roles of the two files being interchanged at the completion of each iteration. The central memory storage connected with this wave function data (about 100 K on $h = \frac{1}{35}$) could be reduced to a small amount proportional to h^{-1} (rather than to h^{-2}) by using random access to store and transfer adjacent geometrical lines of data rather than adjacent planes. During the running of the program it was found essential to use an on-line display to study the convergence of successive $r^{(k)}$, Eq. (42), and successive λ_n, Eq. (8), and also to use sense switches to control the sequence of inner and outer iterations and to apply or recover from the acceleration device.

APPENDIX A. Definitions of Various Quantities

In the following list of definitions ϕ' stands for $d\phi/du$. Quantities not explicitly defined may be obtained by cyclic symmetry. (For example, $\cos\theta_2$ may be obtained from $\cos\theta_1$).

$$\rho = r_{23}r_{31}r_{12}\phi'(u_1)\,\phi'(u_2)\,\phi'(u_3)/4,$$

$$\cos\theta_1 = \frac{-r_{23}^2 + r_{31}^2 + r_{12}^2}{2r_{31}r_{12}},$$

$$R^2 = r_{23}^2 + r_{31}^2 + r_{12}^2 ,$$

$$\Delta = \tfrac{1}{4}[(r_{23} + r_{31} + r_{12})(-r_{23} + r_{31} + r_{12})$$
$$(r_{23} - r_{31} + r_{12})(r_{23} + r_{31} - r_{12})]^{1/2},$$

$$\cos\lambda = 4.3^{1/2}\Delta/R^2,$$

$$F = 3^{-1/2}(r_{23}^2 + r_{31}^2 - 2r_{12}^2),$$

$$G = r_{23}^2 - r_{31}^2 ,$$

$$\sigma_1 = -\frac{r_{31}^2 - r_{12}^2}{r_{23}} + \frac{r_{12}^2 - r_{23}^2}{r_{31}} + \frac{r_{23}^2 - r_{31}^2}{r_{12}} ,$$

$$\rho g_{11} = 2\phi_2'\phi_3'(3 + \cos\theta_1 - \cos\theta_2 - \cos\theta_3)/\phi_1',$$

$$\rho g_{23} = 2\phi_1'(\cos\theta_1 - 1),$$

$$\rho l_i = 16.3^{-3/2}R^2\sigma_i/\phi_i', \qquad i = 1, 2, 3,$$

$$\rho m_{11} = 8.3^{-1/2}\left\{G\sigma_1 + 4\Delta^2\left(-\frac{2}{r_{12}} - \frac{1}{r_{23}} + \frac{1}{r_{31}}\right)\right\}\Big/\phi_1',$$

$$\rho m_{12} = 8.3^{-1/2}\left\{G\sigma_2 + 4\Delta^2\left(-\frac{2}{r_{12}} + \frac{1}{r_{23}} + \frac{1}{r_{31}}\right)\right\}\Big/\phi_2',$$

$$\rho m_{13} = 8.3^{-1/2}\left\{G\sigma_3 + 4\Delta^2\left(+\frac{2}{r_{12}} + \frac{1}{r_{23}} + \frac{1}{r_{31}}\right)\right\}\Big/\phi_3',$$

$$\rho m_{21} = -8.3^{-1/2}\left\{F\sigma_1 + 4.3^{1/2}\Delta^2\left(+\frac{1}{r_{23}} + \frac{1}{r_{31}}\right)\right\}\Big/\phi_1',$$

$$\rho m_{22} = -8.3^{-1/2}\left\{F\sigma_2 + 4.3^{1/2}\Delta^2\left(-\frac{1}{r_{23}} - \frac{1}{r_{31}}\right)\right\}\Big/\phi_2',$$

$$\rho m_{23} = -8.3^{-1/2}\left\{F\sigma_3 + 4.3^{1/2}\Delta^2\left(-\frac{1}{r_{23}} + \frac{1}{r_{31}}\right)\right\}\Big/\phi_3',$$

$$N_0 = R^4(1/3 + \sin^2\lambda), \qquad N_1 = 4/3FR^2,$$

$$N_2 = 4/3GR^2, \qquad N_3 = 4/3(G^2 - F^2), \qquad N_4 = 8/3FG,$$

$$N_5 = R^4(2/3 - 2/9\sin^2\lambda), \qquad d_0 = N_0 , \qquad d_1 = N_1 ,$$

$$d_2 = N_2 , \qquad d_3 = \tfrac{1}{2}N_4 , \qquad d_4 = \tfrac{1}{2}(N_5 + N_3),$$

$$d_5 = \tfrac{1}{2}(N_5 - N_3).$$

APPENDIX B. SYMMETRY REDUCTIONS IN THE NUMERICAL PROBLEM

This appendix describes how the transpose and permutation symmetries, Eqs. (24) and (25), may be exploited to cut down the size of the relaxation problem, using the nine-state central and tensor problem as an example.

1. *Permutation Symmetry*

Permutation symmetry may be used to confine the solution of the inhomogeneous equations (7, 33) (or homogeneous equations (9) in the zero RHS scheme) to one of the six tetrahedra making up the cube, thereby reducing storage space and computing time by a factor of about six. The basic tetrahedron T is taken to be the one containing the points $P(i, j, k)$ with $k \leqslant i \leqslant j$. The cube of mesh points may be considered to be the union of disjoint sets $\mathscr{S}(P)$, P in T, containing the points $P_i = R_i P$, $i = 1, 2,..., 6$, which transform into one another under the action of the six permutation operators $R_1 = e$, $R_2 = (13)$, $R_3 = (123)$, $R_4 = (23)$, $R_5 = (132)$, and $R_6 = (12)$. $\mathscr{S}(P)$ contains $w = w(P)$ points lying in the plane through P perpendicular to the principal diagonal of the cube (the line $u_1 = u_2 = u_3$ in Fig. 1) where $w = 6$ if none of the indices i, j, and k are equal, $w = 3$, if a pair of indices are equal, and $w = 1$ if all of the indices are equal. The values of a symmetric vector ψ at the points P_i are related by

$$\psi(P_i) = R_i \psi(P), \qquad i = 1, 2,..., 6, \tag{B1.1}$$

where $\psi(P)$ and $\psi(P_i)$ are nine component vectors and R_i is a 9×9 permutation matrix representing the permutation operator R_i and defined in Section 2B.

The permutation symmetry of H, Eq. (25), implies that if a symmetric vector satisfying (B1.1) at all points is substituted into the inhomogeneous equations (33), then the w(block) equations belonging to points in a particular set $\mathscr{S}$ are all identical with one another (after factors of permutation matrices are cancelled out on both sides of each equation). However, the symmetry of the vector is not preserved in an SOR process where individual lines of data belonging to individual points in $\mathscr{S}$(each line containing nine wavefunction values) are updated separately from one another as individual steps in a process including all the internal points of the cube outside the hard core. This is because of the progressive property of SOR that the result of an individual step depends on the ordering of previous steps. But the permutation symmetry of the vector is preserved in an SOR process where all the wavefunction values at all the points in a set $\mathscr{S}$ (forming an extended "line") are updated simultaneously in a single step, and so treated equally with respect to permutation symmetry. In this case the identity of the w equations implies that the relaxation problem separates into six identical subproblems of SOR by lines over a tetrahedron as defined in Section 5, Eqs. (34–36).

The subproblem connected with T may be made self-contained in the sense of containing no references to points outside T. Where the SOR equation (34) belonging to a particular point P in T contains couplings to points P' in $\mathcal{N}(P)$ outside T the contribution of such points may be included by reflecting them back into points P'' within T and making appropriate modifications to the coefficients $H_{PP''}$. Dividing $\mathcal{N}(P)$ into the set $\mathcal{I}(P)$ of points P'' internal to T and the set $\mathcal{E}(P)$ of points P' external to T, it is found that eight different cases of such coupling to points in $\mathcal{E}(P)$ occur (depending on the position of P with respect to the boundary of T) and that, in all cases where $\mathcal{E}(P)$ is not empty, the points in $\mathcal{E}(P)$ reflect back into $\mathcal{I}(P)$ [40]. For example, if $P = (j, j, k)$, $P' = (j + 1, j, k)$, and $P'' = (j, j + 1, k)$ (corresponding to $r = 13$, 1, and 2 in Table VIII, respectively), then $H_{PP''}$ may be replaced by $H_{PP''} + H_{PP'} R_6$, and reference to P' omitted.

In the resulting modified finite difference matrix H^M transpose symmetry is not preserved near the boundaries of the tetrahedron. A transpose symmetric matrix $w H^M S$ for use in the subproblem may be obtained from H^M by means of two operations (not affecting SOR): First, left-multiply both sides of the matrix equation defining the eigenvalue–eigenvector subproblem by a diagonal matrix whose elements pertaining to P are all equal to $w(P)$; second, replace ψ on both sides by $S\psi(=\psi)$ where the projector $S(=S^2)$ is a block diagonal, transpose symmetric, and singular matrix whose block pertaining to P is $\sum_i' R_i / \sum_i' 1$, primed summation restricting i such that $R_i P = P$. That $w H^M S$ is symmetric can be demonstrated by considering particular cases. For example, with P, P', and P'' defined as above, the equality of $(w H^M S)(P, P'') = w(P) H^M(P, P'') S(P'') = 3 \cdot (H(P, P'') + H(P, P') R_6) \cdot 1$ with $[(w H^M S)(P'', P)]^T = S(P)(H(P'', P))^T w(P'') = \frac{1}{2}(1 + R_6) \cdot H(P, P'') \cdot 6 = 3(H(P, P'') + R_6 H(P, P''))$ is conditional upon the equality of $H(P, P') R_6$ with $R_6 H(P, P'')$, and this follows from (25) by writing $H(P, P') R_6 = H(R_6 P, R_6 P'') R_6 = (R_6 H(P, P'') R_6^{-1}) R_6 = R_6 H(P, P'')$. The singularity connected with S may be removed by changing to a basis that diagonalizes S to a matrix of ones and zeros (with $w H^M$ simultaneously undergoing the appropriate similarity transformation) and by omitting those equations connected with the zeros.

Some of the above points can be illustrated with the simple two-dimensional problem of Fig. 8 defined by the four inhomogeneous equations

$$
\begin{aligned}
H_{11}\psi_1 + H_{12}\psi_2 + H_{13}\psi_3 + H_{14}\psi_4 &= \theta_1 , \\
H_{21}\psi_1 + H_{22}\psi_2 + H_{23}\psi_3 + H_{24}\psi_4 &= \theta_2 , \\
H_{31}\psi_1 + H_{32}\psi_2 + H_{33}\psi_3 + H_{34}\psi_4 &= \theta_3 , \\
H_{41}\psi_1 + H_{42}\psi_2 + H_{43}\psi_3 + H_{44}\psi_4 &= \theta_4 ,
\end{aligned}
$$

pertaining to the square. Assuming permutation symmetry about the main diagonal of the square, ψ_1 may be replaced by $R\psi_4$ in the last three equations (where if ψ_i

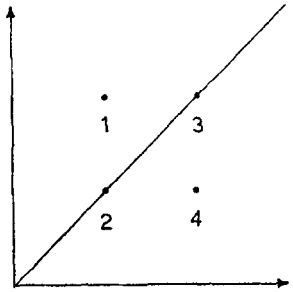

FIG. 8. Two-dimensional problem with permutation symmetry about the line through points 2 and 3.

has a number of components, either symmetric or antisymmetric, then R is a permutation matrix) thereby defining a subproblem with three modified equations

$$H_{22}\psi_2 + H_{23}\psi_3 + (H_{24} + H_{21}R)\,\psi_4 = \theta_2\,,$$
$$H_{32}\psi_2 + H_{33}\psi_3 + (H_{34} + H_{31}R)\,\psi_4 = \theta_3\,,$$
$$H_{42}\psi_2 + H_{43}\psi_3 + (H_{44} + H_{41}R)\,\psi_4 = \theta_4\,,$$

pertaining to the lower triangle. The matrix

$$wH^{MS} = \begin{pmatrix} H_{22}\cdot\tfrac{1}{2}(1+R) & H_{23}\cdot\tfrac{1}{2}(1+R) & H_{24}+H_{21}R \\ H_{32}\cdot\tfrac{1}{2}(1+R) & H_{33}\cdot\tfrac{1}{2}(1+R) & H_{34}+H_{31}R \\ 2H_{42}\cdot\tfrac{1}{2}(1+R) & 2H_{43}\cdot\tfrac{1}{2}(1+R) & 2(H_{44}+H_{41}R) \end{pmatrix},$$

is transpose symmetric, e.g., $(2H_{42}\cdot\tfrac{1}{2}(1+R))^T = H_{24} + RH_{24} = H_{24} + R(R^{-1}H_{21}R) = H_{24} + H_{21}R$.

For a group-theoretical analysis of symmetry reductions in numerical problems (see [30]).

2. *Transpose Symmetry*

Transpose symmetry makes it possible to avoid using data from the lower half of H thereby roughly halving the total peripheral storage and processing time which is almost completely connected with handling the coefficient data. The coefficient blocks $H_{PP'}$ needed at the Pth step of SOR, Eq. (34), are read into central memory at that step, and the wavefunction data needed is made available by accessing an array containing three adjacent planes of ψ. It is not necessary to compute all the contributions $H_{PP'}\,\psi_{P'}$ to eq. (34) at the Pth step; those contributions from points $P' < P$ may be computed at the (P')th steps as $(H_{P'P})^T\,\psi_P^{(k+1)}$ (as soon as $\psi_{P'}$ has been updated), using transpose symmetry, Eq. (24). If these contributions are

successively stored in the Pth location of an auxiliary vector η then Eq. (34) may be replaced by

$$\eta_P + B_P \psi_P^{(k+(1/2))} + \sum_{P'>P} H_{PP'} \psi_{P'}^{(k)} = (\rho N \psi_n)_P , \tag{B2.1}$$

where

$$\eta_P = \sum_{P'<P} (H_{P'P})^T \psi_{P'}^{(k+1)}. \tag{B2.2}$$

As soon as ψ_P has been updated its contribution,

$$(H_{PP'})^T \psi_P^{(k+1)}, \tag{B2.3}$$

to the $\eta_{P'}$ associated with the steps $P' > P$ may be computed. It is clear that at each step of an SOR procedure incorporating this symmetry saving the arithmetic involved, i.e., that connected with Eqs. (B2.1) and (B.2.3), uses data only from the upper half of H.

ACKNOWLEDGMENTS

It is a pleasure to acknowledge the assistance of the following individuals and institutions: Professor H. Messel, and the Science Foundation for Physics within the University of Sydney, for the provision of excellent research facilities and for support with computing; Professor S. T. Butler, Head of the Department of Theoretical Physics, Sydney University, for interest and support connected with computing; Professor I. E. McCarthy of Flinders University, Professors H. Green and C. A. Hurst of the University of Adelaide, and Professor B. H. J. McKellar of the University of Melbourne, for hospitality, and support with computing; Professor N. Austern and B. H. J. McKellar and Drs. B. Davies, R. Hewitt, C. Pask, J. Winings, and A. Bromley, for interest and advice; the staffs and managements of the computing centers at the Universities of Sydney, Adelaide, and Melbourne, and at the Australian Taxation Department, Canberra; The Australian Research Grants Commission for the provision of grants for computing; and Imperial Chemical Industries of Australia and New Zealand and the University of Sydney for the award of research scholarships to B. R. E. Lederer, and the Australian Government for the award of a Commonwealth Postgraduate Studentship to G. C. Vorlicek.

REFERENCES

1. D. M. BRINK AND R. E. PEIERLS, *Comm. Nucl. Particle Phys.* **1** (1968), 92.
2. L. M. DELVES, *in* "Proceedings of the Symposium on Light Nuclei," Bresla, Yugoslavia, 1967, p. 158. Gordon and Breach Science Publishers, London, 1968.
3. L. M. DELVES AND A. C. PHILLIPS, *Rev. Mod. Phys.* **41** (1969), 497.
4. R. V. REID, *Ann. Phys.* (*N.Y.*) **50** (1968), 411.
5. M. A. HENNELL AND L. M. DELVES, *Phys. Lett.* **40B** (1972), 20.

6. A. D. JACKSON, A. LANDE, AND P. U. SAUER, *Phys. Lett.* **35B** (1971), 365.
7. M. R. STRAYER AND P. U. SAUER, *Nucl. Phys. A* **231** (1974), 1.
8. J. BRUINSMA AND R. VAN WAGENINGEN, *Phys. Lett.* **44B** (1973), 221.
9. V. F. DENIM AND YU. E. POKROVSKY, *Phys. Lett.* **47B** (1973), 394.
10. R. A. BRANDENBURG AND Y. E. KIM, *Phys. Lett.* **49B** (1974), 205.
11. A. LAVERNE AND C. GIGNOUX, *Nucl. Phys. A* **203** (1973), 597.
12. S. C. BHATT, J. S. LEVINGER, AND E. HARMS, *Phys. Lett.* **40B** (1972), 23.
13. I. R. AFNAN AND J. M. READ, *Phys. Rev.* **C8** (1973), 1294.
14. T. HAMADA AND I. D. JOHNSTON, *Nucl. Phys.* **34** (1962), 382.
15. L. M. DELVES AND M. A. HENNELL, *Nucl. Phys. A* **168** (1971), 347.
16. CHI-YU HU, *Phys. Rev.* **C3** (1971), 2151.
17. I. M. BASSETT AND B. R. E. LEDERER, *Phys. Lett.* **32B** (1970), 550.
18. I. M. BASSETT, B. R. LEDERER, AND G. C. VORLICEK, *Phys. Lett.* **51B** (1974), 329.
19. T. KIKUTA (Ohmura), M. MORITA, AND M. YAMADA, *Prog. Theor. Phys.* **15** (1956), 222.
20. G. C. VORLICEK, Ph. D. thesis, to appear.
21. L. M. DELVES, "Proceedings of the Texas A. & M. Conference," p. 369. Benjamin, New York, 1968.
22. G. DERRICK AND J. M. BLATT, *Nucl. Phys.* **8** (1958), 310.
23. G. H. DERRICK, *Nucl. Phys.* **16** (1960), 405.
24. G. H. DERRICK, *Nucl. Phys.* **18** (1960), 303.
25. E. P. WIGNER, "Group Theory and its Applications to the Quantum Mechanics of Atomic Spectra," Academic Press, New York, 1959.
26. H. C. BOLTON AND H. I. SCOINS, *Proc. Camb. Phil. Soc.* **52** (1956), 215; **53** (1957), 150; I. M. BASSETT, *Austral. J. Phys.* **21** (1968), 113; N. W. WINTER AND W. MCKOY, *Phys. Rev.* **A2** (1970), 49; **A2** (1970), 2219.
27. Y. C. TANG, E. W. SCHMID, AND R. C. HERNDON, *Nucl. Phys.* **65** (1965), 203.
28. L. M. DELVES, *Advan. Nucl. Phys.* **5** (1972), 1.
29. H. A. BETHE AND R. E. BACHER, *Rev. Mod. Phys.* **8** (1936), 82.
30. P. I. RICHARDS, *SIAM Rev.* **5** (1963), 234.
31. B. DAVIES, *Nucl. Phys.* **88** (1966), 361.
32. A. M. OSTROWSKI, *Arch. Rational Mech. Anal.* **1** (1958), 233.
33. G. E. FORSYTHE AND W. R. WASOW, "Finite Difference Methods for Partial Differential Equations," Wiley, New York, 1960.
34. C. L. PEKERIS, *Phys. Rev.* **112** (1958), 1649; A. S. COOLIDGE AND H. M. JAMES, *Phys. Rev.* **51** (1937), 855.
35. E. H. NEVILLE, *J. Indian. Math. Soc.* **20** (1934), 87.
36. Z. KOPAL "Numerical Analysis," Chapman and Hall, London, 1955.
37. L. M. DELVES AND J. M. BLATT, *Nucl. Phys. A* **98** (1967), 503, 507.
38. J. S. LEVINGER, *Springer Tracts Mod. Phys.* **71** (1974), 88.
39. R. S. VARGA "Matrix Iterative Analysis," Prentice-Hall, Englewood Cliffs, New Jersey, 1962.
40. B. LEDERER, Ph. D. thesis, Univ. Sydney, 1975.
41. G. A. BAKER, JR., "Essentials of Padé approximations," Academic Press, New York, 1975.